

**QUANTUM AMPLIFIER VIA QUANTUM RESERVOIR
PROCESSING**

CHOO WEI ZHENG

XIAMEN UNIVERSITY MALAYSIA

2024



XIAMEN UNIVERSITY MALAYSIA

廈門大學 馬來西亞分校

FINAL YEAR PROJECT REPORT/ THESIS OF DEGREE


**QUANTUM AMPLIFIER VIA QUANTUM RESERVOIR
PROCESSING**

NAME OF STUDENT : CHOO WEI ZHENG
STUDENT ID : EEE2004046
SCHOOL/ FACULTY : XIAMEN UNIVERSITY MALAYSIA,
PROGRAMME : BACHELOR OF SCIENCE IN PHYSICS
(HONOURS)
INTAKE : 2020/09
SUPERVISOR : PROF.DR. TOMASZ PATEREK

26 DECEMBER 2023

DECLARATION

I hereby declare that this project/ thesis is based on my original work except for citation and quotations which have been duly acknowledged. I also declare that it has not been previously and concurrently submitted for any other degree or award at Xiamen University Malaysia or other institutions

Signature : 

Name : Choo Wei Zheng

ID No : EE2004046

Date : 28 Dec 2023

APPROVAL FOR SUBMISSION

I certify that this project report/ thesis entitled “**QUANTUM AMPLIFIER VIA QUANTUM RESERVOIR PROCESSING**” that was prepared by CHOO WEI ZHENG has met the required standard for submission in partial fulfillment of the requirements for the award of Bachelor of Science in Physics at Xiamen University Malaysia.

Approved by,

Signature : T. Paterek
Supervisor : Prof. Dr Tomasz Paterek
Date : 20/06/2024

Signature : _____

Co-Supervisor : _____

Date : _____

The copyright of this report belongs to the author under the terms of Xiamen University Malaysia copyright policy. Due acknowledgement shall always be made of the use of any material contained in, or derived from, this project report/ thesis.

© 2024, Choo Wei Zheng. All right reserved.

ACKNOWLEDGEMENTS

I would like to thank all who contributed to the successful completion of this project. I would like to express my gratitude to my research supervisor, Prof. Dr. Tomasz Paterek for his invaluable advice, guidance and his enormous patience throughout the development of the research.

ABSTRACT

In quantum information technologies, qubits represent the basic unit of information. Weak quantum signals require amplification, but the no-cloning theorem limits this process, characterised by the Haus-Caves limit in quantum optics. This thesis explores using a quantum reservoir processor (QRP), a type of quantum neural network, to simulate quantum-limited amplifiers combining the strengths of neural networks and quantum technologies to offer simplicity and versatility. The research demonstrates that QRPs can simulate unitary transformations and general quantum channels, and can implement quantum amplification efficiently, though the current gain is heavily limited.

TABLE OF CONTENT

DECLARATION	ii	
APPROVAL FOR SUBMISSION	iii	
ACKNOWLEDGEMENTS	v	
ABSTRACT	vi	
TABLE OF CONTENTS	vii	
LIST OF TABLES	ix	
LIST OF FIGURES	x	
LIST OF SYMBOLS	xi	
CHAPTER		
1	INTRODUCTION	1
2	LITEARTURE REVIEW	3
	2.1 Quantum Reservoir Processing	3
	2.2 Introduction to quantum amplifier	7
	2.3 Parametric Amplifier	16
3	RESEARCH METHODOLOGY	16
	3.1 Tools	16
	3.1.1 Quantum state	18
	3.1.2 Fidelity between quantum states	18
	3.1.3 Fidelity between unitaries	18
	3.1.4 Quantum operation	19
	3.1.5 Amplitude damping	22
	3.1.6 Fidelity between quantum channels	22
	3.2 Quantum reservoir processor scenario	24
	3.2.1 1-qubit reservoir	24
	3.2.2 2-qubit reservoir	26
	3.3 Optimization algorithm	27
	3.3.1 Training of unitary	27
	3.3.2 Training of channels	27

4	RESULTS	30
	4.1 Implementation of unitary	30
	4.1.1 Simple unitary of operations	30
	4.1.2 Random unitaries	33
	4.1.3 Comparison between 1-qubit and 2-qubit reservoir	34
	4.2 Implementation of channel	36
	4.2.1 Amplitude damping	36
	4.2.2 Random channel	38
	4.3 Implementation of quantum amplifier	39
	4.3.1 Kraus operator for the parametric amplifier	39
	4.3.2 The gain parameter	40
	4.3.3 Fidelity of the amplifier map	40
	4.3.4 Demonstrate that quantum reservoir processor implements quantum-limited amplifier	41
5	DISCUSSION	43
6	CONCLUSION AND RECOMMENDATION	44
	REFERENCES	46

LIST OF TABLES

Table 4.1: The histogram of fidelity of each unitaries of 1-qubit reservoir	41
Table 4.2: The optimization process of simple unitary transformations with the 2-qubit reservoir	43

LIST OF FIGURES

Figure 2.1: The framework quantum network	3
Figure 2.2: Amplification and introduces the tradition ball-and-stick phase-space diagrams	10
Figure 2.3: Simple circuit of parametric amplifier	14
Figure 3.1: Phase space plot of coherent state	17
Figure 3.2: Phase space plot of coherent state	19
Figure 3.3: Single qubit quantum operation	20
Figure 3.4: The framework of the 1-qubit reservoir	24
Figure 3.5: The framework of the 1-qubit reservoir by introducing one more pump	25
Figure 3.6: The framework of the 2-qubit reservoir	26
Figure 3.7: The flow of genetic algorithm	28
Figure 4.1: Pauli matrices and simple gates	30
Figure 4.2: The implementation of genetic algorithm on unitary transformation	32
Figure 4.3: Pauli matrices and simple gates	33
Figure 4.4: Pauli matrices and simple gates	35
Figure 4.5: Pauli matrices and simple gates	35
Figure 4.6: The optimization process of quantum reservoir processor in simulating random quantum channel	36
Figure 4.7: The total iteration of different requirement of accuracy.	37
Figure 4.8: The total iteration of different requirement of accuracy presents the comparison of the computation cost.	38
Figure 4.9: The relationship between different component of the identity.	40
Figure 4.10: The optimization process of QRP in simulating parametric amplifier with $g = 1.001$	41
Figure 4.11: The optimization process of QRP in simulating parametric amplifier with $g = 1.005$	41

LIST OF SYMBOLS / ABBREVIATIONS

Symbol	Definition or result [unit]
H	Hamiltonian, [J]
H_R	Hamiltonian of the reservoir, [J]
a	Annihilator operator
a^\dagger	Creation operator
E	Energy level, [J]
P	Pump
J	Coupling
k	Boltzmann constant
T_n	Noise temperature, [°C]
A	Added noise number
G	Gain
\bar{E}	Electric Field
t	Time
F	Fidelity
D	Displacement operator
L	Added noise number
b	Ancillary mode
\mathcal{P}	Projection operator
U	Unitary
\mathcal{P}	Parameter
N	Gaussian
P	Momentum, [kg m/s]
X	Position, [m]
p	Momentum (dimensionless)
x	Position (dimensionless)
ρ	Density matrix
σ_k^x	Pauli-X operator acting on kth qubit
σ_k^y	Pauli-Y operator acting on kth qubit
\hbar	Reduced Planck's constant, [J/s]
ω	Angular frequency, [rad/s]
κ	Coupling strength
x	Hermitian quadrature components of the mode
$ \alpha\rangle$	Coherent state
$ \psi\rangle$	Any quantum state
\mathcal{E}	Completely positive map
$ \psi_{\text{in}}\rangle$	Input state
$ \psi_{\text{ideal}}\rangle$	Desired output state
θ	Scattering angle, [°]
γ	Probability of losing a photon

$ \phi\rangle$	Any quantum state
$ g\rangle$	Ground state
$ e\rangle$	Excited state

CHAPTER 1

INTRODUCTION

In quantum information technologies, the basic unit of information is a quantum bit or a qubit. In some situations, the quantum signal is too weak and hence it is crucial to make the signal stronger, say for transmission along long channels. The no-cloning theorem forbids the exact copying of quantum states and sets limits to how well the signal can be amplified [1]. The corresponding constraints are well known in the field of quantum optics under the name of the Haus-Caves limit [2], but an actual device achieving this limit has not yet been built. Some experimentalist have examined that the upper bound on the total system noise of their device under real operating conditions is three times the quantum limit, by using a newly developed noise source, they achieved a power gain amplification of at least 40 dB [3]. Some quantum circuit experiments have been implemented and the analysis was drawn by compared the experiment with theoretical result, they presented a novel class of quantum-limited amplifiers which operate effectively detuned from any instability [4]. Furthermore, a way to measure phase information in any incoming resource state by using Quantum Neuromorphic Platform have been proposed in Ref [5]. The basic idea of the present thesis is to use a particular information processor appearing in the field of quantum artificial intelligence to simulate the actions of the quantum-limited amplifiers and in this way pave the way toward a physical amplifying device.

The platform to be considered here is called *quantum reservoir processor* [6] and it is a special kind of a quantum neural network (QNN). In general, QNNs represent novel technological advancements that amalgamate the characteristics of artificial neural networks with quantum information technologies [7–9]. Artificial neural networks are computational systems inspired by biological processes, capable of learning from examples to execute intricate tasks, particularly in the realms of "big data" [10–12] machine learning. On the other hand, quantum information technologies harness quantum phenomena for practical purposes such as quantum computation, quantum cryptography, and long-distance quantum communications. The advantages

of quantum reservoir processor (QRP) include its conceptual simplicity [13], where instead of multi-layered optimization of parameters in typical neural networks QRP is optimized over only a single layer, and universality, where a single QRP device is capable of making multiple measurements, preparing various quantum states or performing computations.

In reservoir processing, a randomly connected network known as the reservoir serves as a dynamical processing unit, into which an input signal is fed. Only the readout weights are trained in the QRP, which map the outcomes of simple measurements on the nodes of the reservoir to the desired output in a linear way. Despite its simplicity, the device is theoretically predicted to be versatile, good for hardware implementation, and has already been frequently used for tasks in the classical domain. These include but are not limited to predicting the time evolution of nonlinear dynamics and features of chaotic systems. All these make QRP an ideal candidate for simulations and hardware implementations of quantum amplifiers.

Summing up, the research objective of this project is to explore the feasibility of QRP for the realization of quantum-limited amplifiers. In the following chapters, the theory of the quantum amplifier will be first reviewed and its overall operation from input to output will be clarified. In particular, the description of the amplifier will be presented in terms of quantum channels and Kraus operators. The framework of QRP will then be developed and it will be shown how can it learn and simulate several unitary transformations (with just one Kraus operator), quantum channels (with two Kraus operators), and finally a quantum amplifier. It is found that the QRP is capable of learning *any* unitary transformation on a qubit and *any* quantum channel on a qubit with high efficiency. In the end, it will be shown that the QRP can implement a quantum amplifying process but its gain is for the moment limited.

CHAPTER 2

LITERATURE REVIEW

2.1 Quantum Reservoir Processing

As indicated in the introduction, quantum reservoir processing (QRP) is a versatile tool that will be used in the present project. All QRPs have the same structure, which is illustrated in Fig. 2.1, originally presented in Ref. [14]. The core of QRP is a network of quantum nodes (called the reservoir or QN) that are linked through random interactions, i.e., the couplings are chosen at random and then fixed. This is an advantage because in many practical quantum networks, the couplings cannot be controlled during fabrication, e.g., the coupling between quantum dots depends on their distance, but the latter is hard to control in an experiment. The QN is then prepared once and for all, and we do not interfere with its inner dynamics other than pumping the whole reservoir with coherent or incoherent radiation denoted as P in the figure.

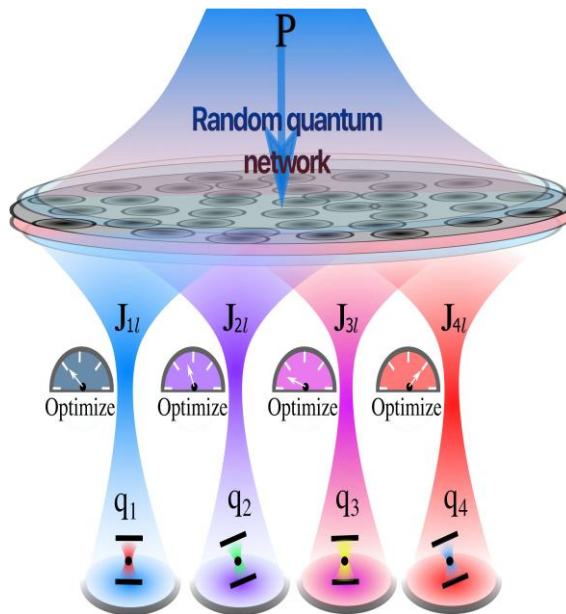


Figure 2.1 A strategy for quantum computing relies on a quantum network, comprised of interconnected nodes represented by black circles. These nodes are stimulated with coherent excitation denoted as P (depicted by a blue arrow). The qubits, labeled as q_k where k ranges from 1 to the total number of qubits, serve as the computational units. Quantum operations on these qubits occur by linking them through the quantum network. The connections between qubits and the network, represented by J_{kl} where l ranges from 1 to the total number of network sites N , form a control layer of tunnelling amplitudes. The varying colors of qubits signify different optimization. Figure from Ref.[12] .

The QN is linked to a set of *computational* qubits where quantum processing takes place. The optimization is permitted only for the coupling strengths between the QN and the computational qubits. Let's give more details about the QRP model. It is assumed that the nodes in QN are two-level quantum systems coupled through quantum tunnelling with arbitrary weights and excited with a classical field. The Hamiltonian is then defined as

$$H_R = \sum_l E_l a_l^\dagger a_l + \sum_{\langle ll' \rangle} K_{ll'} (a_l^\dagger a_{l'} + a_{l'}^\dagger a_l) + \sum_l (P_l^* a_l + P_l a_l^\dagger), \quad (2.1)$$

where the operators a_l^\dagger and a_l represent the raising and lowering operators of a two-level system in the l th node. Specifically, they are expressed by $a_l^\dagger = |e\rangle\langle g|_l$, where $|g\rangle$ and $|e\rangle$ are the ground and excited states respectively of the system with index l . The quantities $K_{ll'}$ and E_l represent nearest-neighbour hopping amplitudes and site-dependent energies. They are chosen randomly within the intervals $[\pm \frac{E_0}{2}]$ and $[\pm \frac{K_0}{2}]$ with suitably chosen E_0 and K_0 . The final term in Eq. (2.1) accounts for the influence of a classical field. For simplicity, a uniform driving is assumed, meaning $P_l = P$ for all sites. All computations are carried out with an open boundary condition, indicating a finite lattice without periodicity, for the quantum network Hamiltonian.

The QN interacts with a set of computational qubits via the coupling weights J_{kl} , and the usual hopping Hamiltonian

$$H = H_R + \sum_{kl} (J_{kl}^* \sigma_k^+ a_l + J_{kl} a_l^\dagger \sigma_k^-), \quad (2.2)$$

where $\sigma_k^\pm = \sigma_k^x \pm i\sigma_k^y$ with σ_k^x and σ_k^y being the Pauli-X and Y operators for the computational qubit q_k . It is worth mentioning that all the interactions between computational qubits occur not directly, but through QN, by adjusting the tunnelling amplitudes J_{kl} for specified times τ .

This and similar QRPs have already been shown to be able to estimate the amount of quantum entanglement and other nonlinear functions of the input state [15], perform quantum state tomography [14], prepare interesting quantum states [16], perform few-qubit quantum computing, and provide metrological advantages [17]. In particular, the setup in Fig. 2.1 has been shown to be capable of implementing a universal set of quantum gates. To this aim, one first chooses a random set of pure states and computes ideal target signal using the target unitary gate. Then the parameters of QRP

Hamiltonian are varied until the output on the computational qubits matches closely the target signal for a random input state. This process is called training and we will describe soon what figures of merit are used to ensure successful training. The final results of this project can be seen as a generalisation of the result in Ref. [14] to any single-qubit unitary and then to any single-qubit channel.

2.2 Introduction to quantum amplifier

Any quantum amplifier must add noise to stay consistent with the no-cloning theorem. A particularly simple class of amplifiers, for which the quantum limits have been thoroughly discussed, is provided by the phase-preserving linear amplifiers. These developments took place in the field of quantum optics and accordingly use the language of continuous variable states. As such a mode of light is represented in the phase space and phase preservation means that the output state of the amplifier is at the same polar angle as the input.

Quantum limits on noise in linear amplifiers

All linear amplifiers, such as *parametric amplifier*, have performance limited by the quantum mechanics. The resulting limit is the minimum value for the noise temperature T_n of the amplifier [18–21]. The noise temperature is described as the increment in input temperature required to account for all the output [22]:

$$T_n \geq \frac{\hbar\omega}{k}, \quad (2.3)$$

where k is Boltzmann constant and $\omega/2\pi$ is the amplifier's input operating frequency. Equation (2.3) means a linear amplifier must add noise to any signal it processes; the added noise must be at least the equivalent of doubling the zero-point noise associated with the input signal.

A linear amplifier is a quantum amplifier whose output signal is linearly related to its input signal. Its definition is very general: such as, both frequency-converting amplifiers, which produce an output frequency different from the input, and phase-sensitive amplifiers, whose response relies significantly on the phase of the input. Importantly, Equation (2.3) applies only to phase-insensitive linear amplifiers.

Fundamental Theorem

For phase insensitive amplifier, the added noise number A satisfies the inequality

$$A \geq \frac{1}{2} |1 \mp G^{-1}|, \quad (2.4)$$

where G is the gain and the upper and lower sign holds for phase-preserving and phase-conjugating amplifiers, respectively. A high-gain phase-insensitive amplifier must add noise to any signal that it proceeds, this statement implied by the fundamental theorem derived below, the added noise must be larger than some value. In contrast, for a phase-preserving device with $G=1$, called “passive”, no additional noise is required. In the following section, A denotes the added noise number, which is the noise added by a phase-insensitive amplifier functioning close to the quantum limit. Particularly, it does not depend on the input signal.

Amplifier uncertainty principle

In phase-sensitive amplifiers, Equation (2.4) is substituted with a broader amplifier uncertainty principle, constraining the product of added noise values for the favoured quadrature phases:

$$A_1 A_2^{\frac{1}{2}} \geq \frac{1}{4} |1 \mp G_1 G_2^{-\frac{1}{2}}|, \quad (2.5)$$

According to the amplifier uncertainty principle, to decrease the noise added to one of the quadrature phases, additional noise is added into another phase. Consider an amplifier with $(G_1 G_2)^{\frac{1}{2}} \gg 1$. If it decreases the noise in one quadrature phase, let say $\Delta X_1 \ll 1/2$, the information of the signal is represented by how much the amplitude of that phase has changed. Furthermore, one can design the amplifier to amplify the phase of interest, which leads to $G_1 \gg 1$, in same phase, the noise is reduced, which means $A_1 \ll \frac{1}{4}$. By utilizing phase-sensitive detection, the amplified signal can be then read out in the selected phase with an accuracy which is much better than the result compare of phase-insensitive way. There is no cheating in quantum mechanics, the noise in another phase will be increased, which leads $\Delta X_2 \gg \frac{1}{2}$, $A_2 \gg \frac{1}{4}$.

The previous section says that as long as quantum amplifier amplified any signal, the added noise must be greater than some value, called the quantum limit. Now, the added noise of a phase-preserving amplifier, referred to as the second moment bound, will

be reviewed. This will be shown in the following section. It is important to study this property before delving into parametric amplifiers, as they satisfy this property.

2.3 Quantum limit on the second moment of added noise

Caves and Joshua argued that there exists fundamental quantum amplifier model, i.e., regardless of how a phase-preserving linear amplifier is realized physically, it is basically the same as a parametric amplifier (but note recent Ref. [23] has proposed a counter example). Hence the details of parametric amplifier are discussed below.

The setting of their investigation is a single bosonic mode, called the primary mode, that undergoes phase-preserving linear amplification. The primary mode has annihilation a and creation operators a^\dagger

$$a = \frac{1}{\sqrt{2}}(x_1 + ix_2), \quad (2.6a)$$

$$a^\dagger = \frac{1}{\sqrt{2}}(x_1 - ix_2), \quad (2.6b)$$

The operators a, a^\dagger satisfy the canonical commutation relation, $[a, a^\dagger] = 1$, or it could be also shown that $[x_1, x_2] = i$. This relationship suggests that the uncertainty principle exist, where $\langle \Delta x_1^2 \rangle \langle \Delta x_2^2 \rangle \geq 1/4$. Here, $\Delta x \equiv x - \langle x \rangle$, and the variance of x is $\langle \Delta x^2 \rangle$.

Equation (2.7) below conceptualizes the signal as a transition through a single-mode field \bar{E} ,

$$\bar{E}(t) = \frac{1}{2}(ae^{-i\omega t} + a^\dagger e^{i\omega t}) = \frac{1}{\sqrt{2}}(x_1 \cos \omega t + x_2 \sin \omega t). \quad (2.7)$$

The annihilation operator a is the complex-amplitude operator for the field. The expectation value of the field, $\langle E(t) \rangle = \text{Re}(\langle a \rangle e^{-i\omega t})$, oscillates with the amplitude and phase of $\langle a \rangle$. The noise in the signal is described by the variance of E . For phase-insensitive noise, its variance keeps constant and is represented by $\langle \Delta E^2 \rangle = \frac{1}{2} \langle |\Delta a|^2 \rangle$. Equation (2.8) represents the symmetric variance of a :

$$\langle |\Delta a|^2 \rangle = \frac{1}{2} \langle \Delta a \Delta a^\dagger + \Delta a^\dagger \Delta a \rangle = \langle |a|^2 \rangle - |\langle a \rangle|^2 \quad (2.8)$$

To represent the symmetric product of a and a^\dagger , we write $|a|^2 = \frac{1}{2}(aa^\dagger + a^\dagger a)$. The uncertainty principle is:

$$\langle |\Delta a|^2 \rangle = \frac{1}{2}(\langle \Delta x_1^2 \rangle + \langle \Delta x_2^2 \rangle) \geq \langle \Delta x_1^2 \rangle^{\frac{1}{2}} \langle \Delta x_2^2 \rangle^{\frac{1}{2}} \geq \frac{1}{2} \quad (2.9)$$

The lower bound is the half-quantum of zero-point (or vacuum) noise. The first inequality is saturated when the noise is insensitive to the phase, that is, meaning that $\langle |\Delta a|^2 \rangle = \langle \Delta x_1^2 \rangle = \langle \Delta x_2^2 \rangle$, and the second inequality is saturated when the uncertainties in quadrature have minimum uncertainty product. Both equalities hold when the mode is in a coherent state $|\alpha\rangle = D(a, \alpha)|0\rangle$. Equation (2.10) represents displacement operator $D(a, \alpha)$ for mode a ,

$$D(a, \alpha) = e^{\alpha a^\dagger - \alpha^* a} = e^{i(\alpha_2 x_1 - \alpha_1 x_2)}, \alpha = \frac{1}{\sqrt{2}}(\alpha_1 + i\alpha_2). \quad (2.10)$$

The phase-preserving linear amplification aim to increase the magnitude of an input signal by a gain g , for any input phase, by adding a minimum noise if possible. Equation (2.11) represents the transformation of the amplification of the expected complex amplitude of the input signal

$$\langle a_{\text{out}} \rangle = g \langle a_{\text{in}} \rangle \quad (2.11)$$

A flawless linear amplifier achieves this while maintaining the signal-to-noise ratio. In the Heisenberg picture, it's not only the expectation value but also the annihilation operator of the primary mode that would transform from input to output.

$$a_{\text{out}} = g a_{\text{in}} \quad (2.12)$$

The second-moment noise would be amplified by the power gain g^2 , that is, $\langle |\Delta a_{\text{out}}|^2 \rangle = g^2 \langle |\Delta a_{\text{in}}|^2 \rangle$. The amplifier's output would be contaminated by the same noise as the input, blown up by a factor of g^2 , but the amplification process would not add any noises to the amplified input noise.

Notice that Caves mentions that there are no perfect phase-preserving linear amplifiers due to the limitation of quantum mechanics. In particular, equation (2.12) does not preserve the canonical commutation relation and therefore violates unitarity. In physical terms, this implies that amplifying the primary mode necessitates its coupling to other physical systems, primarily to supply the energy required for amplification. These additional systems, akin to the internal degrees of freedom of the

amplifier, inevitably introduce noise into the output. Equation (2.13) represents the physical requirement as an input-output relation [24,25],

$$a_{\text{out}} = g a_{\text{in}} + L^\dagger, \quad (2.13)$$

where L is the added-noise operator, which describes the internal degrees of freedom. $\langle L^\dagger \rangle = 0$ is an assumption that usually used to keep the Equation (2.11). The relationship $[L, L^\dagger] = g^2 - 1$ is required in order to preserve the canonical commutation relation between input and output. This implies the uncertainty principle,

$$\langle |\Delta L|^2 \rangle \geq \frac{1}{2} g^2 - 1, \quad (2.14)$$

The amplifier should be able to receive any input in the primary mode. This limits that, before amplification, the internal degrees of freedom and the primary mode cannot be correlated. By summing up the amplified input noise and the noise added by the internal degrees of freedom, leads the total output noise, so that:

$$\langle |\Delta a_{\text{out}}|^2 \rangle = g^2 \langle |\Delta a_{\text{in}}|^2 \rangle + \langle |\Delta L|^2 \rangle. \quad (2.15)$$

The uncertainty principle (2.14) constrains the added noise, and then Eq. (2.9), provides a lower bound for the output noise:

$$\langle |\Delta a_{\text{out}}|^2 \rangle = g^2 - \frac{1}{2}. \quad (2.16)$$

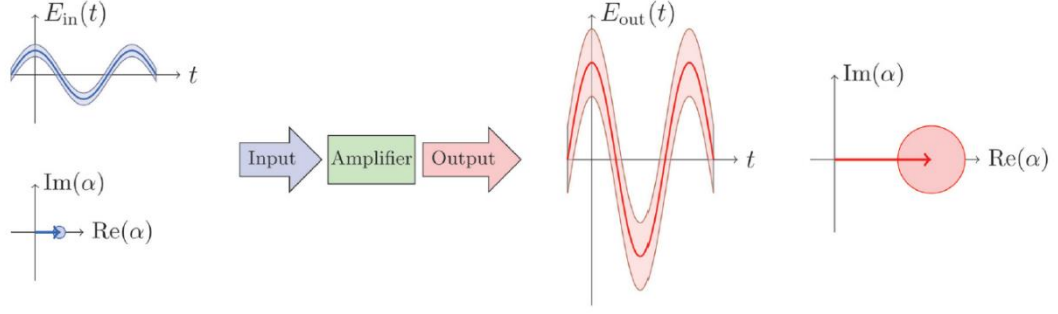


Figure 2.2 The blue color and red color represent input signal $E_{in}(t) = \cos \omega t$ and output signal $\bar{E}_{out}(t) = g \cos \omega t$ for a single-mode. They are the phrase preserving linear amplifier with amplitude gain $g=4$. For both of them, the input and output have the same phase. The input $\langle a_{in} \rangle = \frac{\langle x_1 \rangle}{\sqrt{2}} = 1$, is amplified to an output, $\langle a_{out} \rangle = g$, both of them are complex amplitudes. The (phase-insensitive) noise on signal is represented by smearing out the mean signal into a band with vertical height equal to the uncertainty in the field, $\langle \Delta \bar{E}^2 \rangle^{\frac{1}{2}} = \frac{\langle \Delta a^2 \rangle^{\frac{1}{2}}}{\sqrt{2}}$. If the input is a coherent state, the input band height and output band height are equal to $\frac{1}{2}$ and $\sqrt{(g^2 - \frac{1}{2})/2}$, correspondingly. The same input and output is also represented by the phase-space diagram as the temporal plots. The arrow represents mean complex amplitude, and circle represents the noise which diameter equal to the height of the band in the temporal plot. To obtain the temporal plots, one can rotate the phase-space stick, ball about the origin and projecting onto the real axis.

Figure 2.2 illustrates the amplification of the field \tilde{E} and introduces the traditional ball-and-stick phase-space diagrams that are used to depict the second-moment noise. The output noise takes the form by referring to the input:

$$\frac{\langle |\Delta a_{out}|^2 \rangle}{g^2} = \langle |\Delta a_{in}|^2 \rangle + \frac{\langle |\Delta L|^2 \rangle}{g^2} = \langle |\Delta a_{in}|^2 \rangle + A. \quad (2.17)$$

Here, A is the second-moment added noise, which was denoted as added noise number in previous section. This characterizes the amplifier's performance, and satisfies the quantum limit:

$$A \equiv \frac{\langle |\Delta L|^2 \rangle}{g^2} \geq \frac{1}{2} \left(1 - \frac{1}{g^2} \right) \xrightarrow{g \rightarrow \infty} \frac{1}{2} \quad (2.18)$$

Again, in the limit of high gain, a phase-preserving linear amplifier adds at least half a quantum of noise to the input noise. All three ways measure how well an amplifier works, but have a problem: they're affected by the remaining gain dependence $1 - \frac{1}{g^2}$. Noise temperature and noise figure face an extra issue because they rely on input noise, which means they're not just about the amplifier itself. Besides, noise temperature does not increase in a straight line with added noise for amplifiers that are nearly at the

quantum limit. So, it is better to use a simpler measure of added noise that does not depend on gain.

$$A_1 \equiv \frac{\langle |\Delta L|^2 \rangle}{g^2 - 1} = \frac{A}{1 - \frac{1}{g^2}} \geq \frac{1}{2} \quad (2.19)$$

Hence, the second-moment quantum limit is $A_1 \geq \frac{1}{2}$.

2.3 Parametric Amplifier

The parametric amplifier provides the simplest model for the ideal linear amplifier [26–28], which saturates the *second-moment bound*. Consider the mode a interacts with an ancillary mode $b = y_1 + iy_2$, which is at the vacuum state at the beginning. The entire Hamiltonian is

$$H = \hbar\omega(a^\dagger a + b^\dagger b) + i\hbar\kappa(abe^{2i\omega t} - a^\dagger b^\dagger e^{-2i\omega t}), \quad (2.20)$$

The pairwise creation or destruction of quantum in the two modes are described by the interaction term. The process of pairwise creation or destruction is accompanied by destruction or creation of a quantum in a pump mode with a frequency of 2ω . The pump mode is not explicitly involved in the Hamiltonian due to its existence in a high-amplitude coherent state, and hence it is essentially classical. The amplitude of the pump mode adds to the coupling strength κ , and its time dependence introduces the explicit time dependencies into the Hamiltonian in the form of $e^{\pm 2i\omega t}$.

The Hamiltonian is simplified in the rotating frame as now shown. Consider the Schrodinger equation:

$$i\hbar \frac{\partial}{\partial t} |\psi\rangle = H|\psi\rangle, \quad (2.21)$$

In a new rotating frame where the state is given by $|\psi'\rangle = U|\psi\rangle$, the Schrodinger equation retains its form

$$i\hbar \frac{\partial}{\partial t} |\psi'\rangle = H' |\psi'\rangle, \quad (2.22)$$

If H' satisfies condition now derived:

$$i\hbar \frac{\partial}{\partial t} |\psi\rangle = H|\psi\rangle, \quad (2.23)$$

$$i\hbar \frac{\partial}{\partial t} (U^\dagger |\psi'\rangle) = HU^\dagger |\psi'\rangle, \quad (2.24)$$

$$i\hbar \left(\frac{\partial}{\partial t} U^\dagger \right) |\psi'\rangle + U^\dagger \frac{\partial}{\partial t} |\psi'\rangle = HU^\dagger |\psi'\rangle, \quad (2.25)$$

$$i\hbar U^\dagger \frac{\partial}{\partial t} |\psi'\rangle = HU^\dagger |\psi'\rangle - i\hbar \frac{\partial}{\partial t} U^\dagger |\psi'\rangle, \quad (2.26)$$

$$i\hbar \frac{\partial}{\partial t} |\psi'\rangle = (UHU^\dagger - i\hbar U \frac{\partial}{\partial t} U^\dagger) |\psi'\rangle, \quad (2.27)$$

By Equation (2.22), Equation (2.27) hence become

$$H' = H_I = UHU^\dagger - i\hbar U \frac{\partial}{\partial t} U^\dagger, \quad (2.28)$$

Notice that H' is written as H_I to follow Caves' notation.

To translate Eq. (2.21) to the iteration picture, defined by the unitary $U = e^{i\omega t(a^\dagger a + b^\dagger b)}$, we need the following terms:

$$U a^\dagger a U^\dagger = e^{i\omega a^\dagger a} e^{i\omega b^\dagger b} a^\dagger a e^{-i\omega a^\dagger a} e^{-i\omega b^\dagger b}, \quad (2.29)$$

$$= a^\dagger a, \quad (2.30)$$

similarly,

$$U b^\dagger b U^\dagger = b^\dagger b, \quad (2.31)$$

and

$$U a b U^\dagger = e^{i\omega a^\dagger a} a e^{-i\omega a^\dagger a} e^{i\omega b^\dagger b} b e^{-i\omega b^\dagger b}, \quad (2.32)$$

$$U a b U^\dagger = e^{i\omega(aa^\dagger - 1)t} a e^{-i\omega a^\dagger a} e^{i\omega(bb^\dagger - 1)t} b e^{-i\omega b^\dagger b}, \quad (2.33)$$

$$= e^{-i\omega t} \sum_{n=0}^{\infty} \frac{(i\omega t)^n}{n!} a a^\dagger{}^n a e^{-i\omega a^\dagger a} \times \quad (2.34)$$

$$e^{-i\omega t} \sum_{n=0}^{\infty} \frac{(i\omega t)^n}{n!} b^\dagger b{}^n b e^{-i\omega b^\dagger b},$$

$$= e^{-i\omega t} a \sum_{n=0}^{\infty} \frac{(i\omega t)^n}{n!} a a^\dagger{}^n e^{-i\omega a^\dagger a} \times \quad (2.35)$$

$$e^{-i\omega t} b \sum_{n=0}^{\infty} \frac{(i\omega t)^n}{n!} b^\dagger b{}^n e^{-i\omega b^\dagger b},$$

$$= a e^{-i\omega t} e^{-i\omega t a^\dagger a} e^{-i\omega t a^\dagger a} (b e^{-i\omega t} e^{-i\omega t b^\dagger b} e^{-i\omega t b^\dagger b}), \quad (2.36)$$

$$= a b e^{-2i\omega t}. \quad (2.37)$$

$$U a^\dagger b^\dagger U^\dagger = e^{i\omega a^\dagger a} a^\dagger e^{-i\omega a^\dagger a} e^{i\omega b^\dagger b} b^\dagger e^{-i\omega b^\dagger b}, \quad (2.38)$$

$$= \sum_{n=0}^{\infty} \frac{(i\omega t)^n}{n!} a^\dagger a{}^n a^\dagger e^{-i\omega a^\dagger a} \times \quad (2.39)$$

$$\sum_{n=0}^{\infty} \frac{(i\omega t)^n}{n!} b^\dagger b{}^n b^\dagger e^{-i\omega b^\dagger b},$$

$$= e^{-i\omega t} a^\dagger \sum_{n=0}^{\infty} \frac{(i\omega t)^n}{n!} a a^\dagger{}^n e^{-i\omega a^\dagger a} \times \quad (2.40)$$

$$e^{-i\omega t} b^\dagger \sum_{n=0}^{\infty} \frac{(i\omega t)^n}{n!} b b^\dagger^n e^{-i\omega b^\dagger b t},$$

$$= a^\dagger e^{-i\omega t} e^{-i\omega t a^\dagger a} e^{-i\omega t a^\dagger a} (b^\dagger e^{-i\omega t} e^{-i\omega t b^\dagger b} e^{-i\omega t b^\dagger b}), \quad (2.41)$$

$$= a^\dagger e^{-i\omega t} e^{+i\omega t(a a^\dagger + 1)} e^{-i\omega t a^\dagger a} (b^\dagger e^{-i\omega t} e^{+i\omega t(b b^\dagger + 1)} e^{-i\omega t b^\dagger b}), \quad (2.42)$$

$$= a^\dagger e^{i\omega t} b^\dagger e^{i\omega t}, \quad (2.43)$$

$$= a^\dagger b^\dagger e^{2i\omega t}. \quad (2.44)$$

$$U \frac{\partial}{\partial t} U^\dagger = e^{i\omega t(a^\dagger a + b^\dagger b)} \frac{\partial}{\partial t} e^{-i\omega t(a^\dagger a + b^\dagger b)}, \quad (2.45)$$

$$= e^{i\omega t(a^\dagger a + b^\dagger b)} (-i\omega(a^\dagger a + b^\dagger b)) e^{-i\omega t(a^\dagger a + b^\dagger b)}, \quad (2.46)$$

$$= -i\omega[U(a^\dagger a + b^\dagger b)U^\dagger], \quad (2.47)$$

$$= -i\omega[a^\dagger a + b^\dagger b]. \quad (2.48)$$

$$UHU^\dagger = U \hbar\omega a^\dagger a + b^\dagger b U^\dagger + U i\hbar k a b e^{2i\omega t} - a^\dagger b^\dagger e^{-2i\omega t} U^\dagger, \quad (2.49)$$

$$= \hbar\omega a^\dagger a + b^\dagger b + i\hbar k e^{2i\omega t} U a b U^\dagger - i\hbar k e^{-2i\omega t} U a^\dagger b^\dagger U^\dagger, \quad (2.50)$$

$$= \hbar\omega a^\dagger a + b^\dagger b + i\hbar k e^{2i\omega t} a b e^{-2i\omega t} - i\hbar k e^{-2i\omega t} (a^\dagger b^\dagger e^{2i\omega t}), \quad (2.51)$$

$$= \hbar\omega a^\dagger a + b^\dagger b + i\hbar k a b - a^\dagger b^\dagger. \quad (2.52)$$

Then

$$H_I = UHU^\dagger - i\hbar U \frac{\partial}{\partial t} U^\dagger, \quad (2.53)$$

$$H_I = \hbar\omega a^\dagger a + b^\dagger b + i\hbar k a b - a^\dagger b^\dagger - i\hbar [-i\omega(ab - a^\dagger b^\dagger)]. \quad (2.54)$$

Therefore

$$H_I = i\hbar k a b - a^\dagger b^\dagger, \quad (2.55)$$

$$i\hbar \frac{\partial}{\partial t} |\psi'\rangle = H_I |\psi'\rangle. \quad (2.56)$$

which can be integrated to give an evolution operator [23]:

$$U_I(t) = e^{-iH_I t/\hbar} \quad (2.57)$$

$$= \exp[r(ab - a^\dagger b^\dagger)], \quad (2.58)$$

$$U_I(t) = \exp[ir(x_1 y_2 - x_2 y_1)] \equiv S(t), r = \kappa t. \quad (2.59)$$

Here, $S(r)$ represents the two-mode squeezing operator [28-31]. In the Heisenberg picture, the annihilation operator of the primary mode undergoes the transformation

$$a_{\text{out}} = S^\dagger a S = a \cosh r - b^\dagger \sinh r = g a - b^\dagger \sqrt{g^2 - 1}. \quad (2.60)$$

In other words, one can say that the output is amplified by taking the form as Equation (2.13) with a gain $g = \cosh r$ and noise operator $L = -b \sinh r = -b \sqrt{g^2 - 1}$ as compared to the input. When the ancillary mode is set up to be started in the vacuum state $|0\rangle$, the noise operator reaches the second-moment bound, resulting in an ideal linear amplifier [27].

To describe the evolution in the interaction picture in detail, taking into account the initial state ρ of the primary mode and the ancillary mode commencing in a vacuum state, the state of the primary mode after the amplification process is:

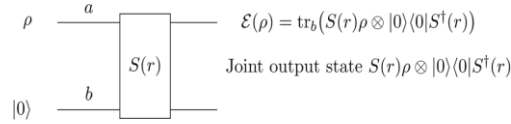


Figure 2.3 A parametric amplifier is implemented to function as an optimal phase-preserving linear amplifier. The principal mode, labelled as a , engages in a two-mode squeezing interaction with an ancillary mode b , which is initially in the vacuum state $|0\rangle$. The resulting amplified output state $\mathcal{E}(\rho)$ of the primary mode is raised up with an amplitude gain $g = \cosh r$, while introducing the minimum allowable quantum-mechanical noise.

$$\mathcal{E} \rho = \text{tr}_b[S(r)\rho \otimes |0\rangle\langle 0|S^\dagger(r)]. \quad (2.61)$$

In this context, \mathcal{E} represents a trace-preserving quantum operation (a completely positive map). This is describing the transformation of the state of the primary mode from the input to the output that undergoes the amplification. The basic quantum circuit of an ideal parametric amplifier is illustrated by Figure 2.3.

Let's first work out $\langle \alpha | S(r) | 0 \rangle$, which is the operator acts on a . From Ref [29], one gets

$$S(r) = \frac{1}{g} e^{-a^\dagger b^\dagger \tanh r} g^{-(a^\dagger a + b^\dagger b)} e^{ab \tanh r}, \quad (2.62)$$

$$S(r) = \frac{1}{g} g^{-a^\dagger a} e^{-a^\dagger b^\dagger \sinh r} e^{ab \sinh r} g^{-b^\dagger b}. \quad (2.63)$$

Then

$${}_b \langle \alpha | S_{ab}(r) | 0 \rangle_b = \frac{1}{g} g^{-a^\dagger a} {}_b \langle \alpha | e^{-a^\dagger b^\dagger \sinh r} e^{ab \sinh r} \times g^{-b^\dagger b} | 0 \rangle, \quad (2.64)$$

Using

$$b^\dagger b|n\rangle = n|n\rangle, \quad (2.65)$$

$$b|0\rangle = 0, \quad (2.66)$$

$$\langle\alpha|b^\dagger = \alpha^*\langle\alpha|, \quad (2.67)$$

one finds

$$g^{-b^\dagger b}|0\rangle = g^0|0\rangle = |0\rangle, \quad (2.68)$$

$$e^{absinh r}|0\rangle = e^0|0\rangle = |0\rangle, \quad (2.69)$$

$$\langle\alpha|e^{-a^\dagger b^\dagger \sinh r} = \langle\alpha|e^{-a^\dagger \alpha^* \sinh r}, \quad (2.70)$$

and

$${}_b\langle\alpha|S_{ab}(r)|0\rangle_b = \frac{1}{g}g^{-a^\dagger a}e^{-a^\dagger \alpha^* \sinh r}\langle\alpha|0\rangle. \quad (2.71)$$

Since $\langle\alpha|0\rangle = e^{-\frac{|\alpha|^2}{2}}$ and $\cosh r = g$:

$$\langle\alpha|S(r)|0\rangle = \frac{1}{g}g^{-a^\dagger a}e^{-a^\dagger \alpha^* \sqrt{g^2-1}}e^{-\frac{|\alpha|^2}{2}} \equiv \sqrt{\pi} K_\alpha \quad (2.72)$$

In this way we obtain a Kraus decomposition of \mathcal{E} where the operators K_α are called Kraus operators [30,31], and act only on the primary mode. An alternative decomposition of \mathcal{E} [32] can be obtained by examining the partial matrix elements of the squeezing operator using the number basis of mode b:

$$\langle n|S(r)|0\rangle = \frac{-1}{g^2} \frac{(g^2-1)^{n/2}}{\sqrt{n!}} g^{-a^\dagger a} (a^\dagger)^n \equiv K_n, \quad (2.73)$$

Performing the trace in Equation (2.61) in the number basis of the ancillary mode provides the Kraus decomposition

$$\mathcal{E}(\rho) = \sum_{n=0}^{\infty} \langle n|S|0\rangle \rho \langle 0|S^\dagger|n\rangle = \sum_{n=0}^{\infty} K_n \rho K_n^\dagger. \quad (2.74)$$

In the later parts of this thesis, this decomposition will be utilized to implement parametric amplifier via quantum reservoir processing.

CHAPTER 3

RESEARCH METHODOLOGY

3.1 Tools

3.1.1 Quantum states

In quantum physics, a quantum state is a mathematical representation of a quantum system's configuration. A coherent state is a specific type of quantum state for the quantum harmonic oscillator, known for its dynamics that closely mimic the behavior of a classical harmonic oscillator. In amplification, coherent states are the natural input states, for which the theory is well developed.

Coherent State

A coherent state describes a single quantum particle such as a single atom or photon, that behaves metaphorically like a swinging pendulum in the quantum world. In quantum mechanics, a coherent state $|\alpha\rangle$ is defined as an eigenstate of the annihilation operator with an eigenvalue α :

$$a|\alpha\rangle = \alpha|\alpha\rangle, \quad (3.1)$$

Since a is not Hermitian, α is complex and can be written as $\alpha = |\alpha| e^{i\theta}$, where $|\alpha|$ and θ represent the amplitude and phase of the state $|\alpha\rangle$ respectively.

Recall the dimensionless variables P and X of momentum and position in quantum mechanics are

$$p^2 = \frac{P^2}{m\hbar\omega}, \quad (3.2)$$

$$x^2 = \frac{m\omega X^2}{\hbar}, \quad (3.3)$$

And the corresponding annihilation operator and the creation operator are

$$a = \frac{1}{\sqrt{2}}(x + ip), \quad (3.4)$$

$$a^\dagger = \frac{1}{\sqrt{2}}(x - ip), \quad (3.5)$$

By linking these two equations, leads

$$X = \frac{1}{\sqrt{2}}(a^\dagger + a), \quad (3.6)$$

$$P = \frac{i}{\sqrt{2}}(a^\dagger - a), \quad (3.7)$$

By calculating the uncertainty of dimensionless position and momentum, which are

$$\Delta X = \sqrt{\langle \alpha | X^2 | \alpha \rangle - \langle \alpha | X | \alpha \rangle^2} \text{ and } \Delta P = \sqrt{\langle \alpha | P^2 | \alpha \rangle - \langle \alpha | P | \alpha \rangle^2},$$

$$\Delta X \Delta P = \frac{1}{2} \langle \alpha | a a^\dagger | \alpha \rangle - \frac{1}{2} |\alpha|^2 \quad (3.8)$$

$$= \frac{1}{2} \langle \alpha | a a^\dagger | \alpha \rangle - \frac{1}{2} \langle \alpha | a^\dagger a | \alpha \rangle \quad (3.9)$$

$$= \frac{1}{2} \langle \alpha | \alpha \rangle [a, a^\dagger]. \quad (3.10)$$

Since $[a, a^\dagger] = 1$, then

$$\Delta X \Delta P = \frac{1}{2} \forall \alpha = \mathbb{C}, \quad (3.11)$$

i.e. the uncertainty relation is saturated. In other words, the coherent states are the minimum uncertainty states.

As shown in figure 3.1, the uncertainty is evenly distributed in all directions, represented by a disk with a diameter of $1/2$. If this state evolves under harmonic

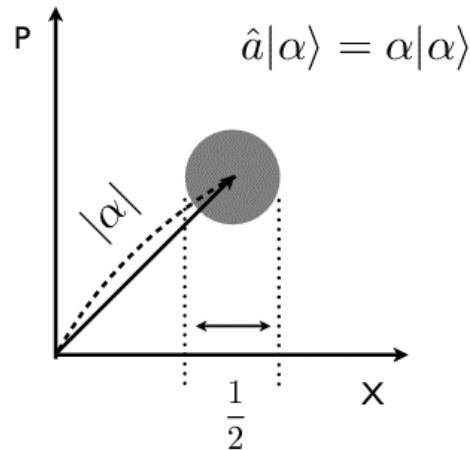


Figure 3.1 The phase space plot of a coherent state illustrates that uncertainty in such a state is uniformly distributed in all directions. The horizontal and vertical axes represent the X and P quadratures of the field, respectively.

oscillator potential, it rotates about the origin without any spread. This is why it is

called to be “as close to classical as possible” as the classical oscillator will do the same, but will be represented by a point instead of the circle.

3.1.2 Fidelity between quantum states

Fidelity is used as an indicator of the similarity between two states. In this thesis we will compare the ideal target state, e.g. obtained by applying a desired unitary to any input state $|\psi_{\text{ideal}}\rangle = U_q|\psi_{\text{in}}\rangle$, to the state produced by the QRP implementation. Let us denote the output state of the QRP machine as ρ_q . The most common fidelity quantifier is defined as follows:

$$F = \langle \psi_{\text{ideal}} | \rho_q | \psi_{\text{ideal}} \rangle \quad (3.12)$$

A general quantum map will also be encountered instead of unitaries. In this case the ideal output is a mixed quantum state, let's say state ρ_1 , and the output of the QRP processor is a potentially different mixed state ρ_2 . The fidelity between two density matrices is commonly defined as [33]:

$$F(\rho_1, \rho_2) = \left(\text{tr} \sqrt{\sqrt{\rho_1} \rho_2 \sqrt{\rho_1}} \right)^2 \quad (3.13)$$

The square roots in this expression are well-defined because both ρ_1 and $\sqrt{\rho_1} \rho_2 \sqrt{\rho_1}$ are positive semidefinite matrices, and the square root of a positive semidefinite matrix is defined via the spectral theorem. One may wonder why this equation is so much more complicated as compared with Equation (3.12). The reason is that we want a function which is equal to 1 if the two density matrices are the same. The set of postulates that any fidelity measure should satisfy was first proposed in [29] and recently reviewed [30]. Last, but not least, in fact Equation (3.12) is just a special case of Eq. (3.13) as one verifies that it reduces to the former for ρ_1 being a pure state.

3.1.3 Fidelity between unitaries

Up to now we have described the fidelity between quantum states. Yet, the main goal of this thesis is to implement certain target operations. For this reason we now review fidelity measures between quantum operations, beginning with the unitary operations. The basic idea is to randomly sample the input state for operations to be compared and take as fidelity for operations the average fidelity between the output states. In some

cases, e.g. unitaries, the resulting expressions can be written in closed form as we now present.

Consider two states $|\psi_a\rangle = U_a|\psi\rangle$ and $|\psi_b\rangle = U_b|\psi\rangle$, which are the results of applying unitaries U_a and U_b on a random initial state $|\psi\rangle$.

TODO: formula missing

Before presenting the fidelity between more general operations than unitaries, a brief introduction to quantum channels and general quantum maps is given.

3.1.4 Quantum Operation

The quantum operation formalism is a standard way to describe the evolution of a quantum system in any situation. The general quantum states are described by the density operator (density matrix) ρ , the properties of which the reader finds in [30]. The transformations between quantum states take the form of a mapping from the input to output density matrix:

$$\rho' = \mathcal{E}(\rho) \tag{3.14}$$

The map \mathcal{E} in this equation is called a quantum operation. Simple examples can be found in Ref [30]. The dynamic change of a state is captured by the quantum operation which occurs as the result of some physical process. Initially, ρ is the state before the process, or say to be input to any quantum channel, and $\mathcal{E}(\rho)$ is the final state after the process happens, or output by the quantum channel, possibly up to some normalization factor.

Environments and quantum operations

Quantum operations naturally occur in the description of open quantum systems. A unitary transformation describes the dynamics of a closed quantum system. It can be imagined that the unitary is a box, which allows the input state and has an output. This

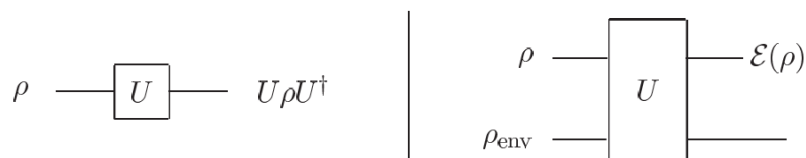


Figure 3.2 The left-hand-side illustrates the model of closed quantum system. The right-hand-side illustrates the model of open quantum systems, which consist of two parts, such as the principal system and an environment.

idea is illustrated on the left-hand side of Fig. 3.2. In this section, the internal framework of the box is not concerned, it could be just constructed with some quantum circuit, or by some Hamiltonian system, or anything else, but of course in next sections some types of boxes which are interesting will be discussed case by case.

A common approach to characterize the behaviour of an open quantum system is to view it as the result of an interaction between two entities: the principal system, representing the system of interest, and an environment. Together, they constitute a closed quantum system, depicted on the right side of Fig. 3.2. Alternatively, suppose a system in a state ρ is input into a box which is coupled to an environment. Generally, the output state $\mathcal{E}(\rho)$ of the system may not be just a simple unitary transformation of the initial state ρ . For now, the system-environment input state is assumed as a product state, $\rho \otimes \rho_{\text{env}}$. Once the environment no longer affects with the box's transformation (denoted by U), a partial trace is to be performed over the environment to get the reduced state of the principal system alone:

$$\mathcal{E}(\rho) = \text{tr}_{\text{env}}[U\mathcal{E}(\rho \otimes \rho_{\text{env}})U^\dagger] \quad (3.15)$$

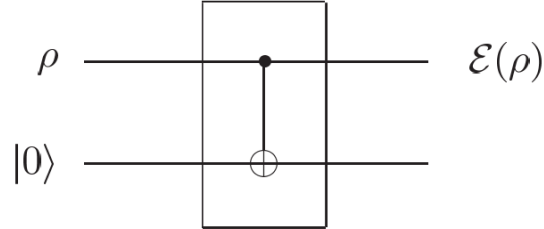


Figure 3.3 The controlled-NOT gate as an elementary example of a quantum operation on the principal system (upper one in the figure).

To show an example of the last equation in action, look at the circuit presented in Fig. 3.3. U is a controlled-NOT gate, with the principal system the control qubit, and the environment initially in the state $\rho_{\text{env}} = |0\rangle\langle 0|$ as the target qubit. Substitute this into Equation (3.15), to obtain

$$\mathcal{E}(\rho) = \mathcal{P}_0\rho\mathcal{P}_0 + \mathcal{P}_1\rho\mathcal{P}_1, \quad (3.16)$$

where $\mathcal{P}_0 = |0\rangle\langle 0|$ and $\mathcal{P}_1 = |1\rangle\langle 1|$ are projection operators. It is seen that this dynamic happens due to the environment which stays in the $|0\rangle$ state only when the system is in $|0\rangle$. If not, the environment is going to be flipped to the state $|1\rangle$.

The derivation of this equation provides an example of the operator-sum representation.

Operator-sum representation

Operator-sum representation gives an elegant form of the quantum operations, which is the re-statement of the Equation (3.15) in terms of operators on the principal system's Hilbert space alone. Let $|e_k\rangle$ be an orthonormal basis for the state space of the environment, and let $\rho_{\text{env}} = |e_0\rangle\langle e_0|$ be the initial state of the environment. Basically, it does not really matter if the environment is starting in a pure or mixed state. If it starts mixed, add an ancillary system to make it pure. Even though this extra system is not real, it does not change how the main system behaves, so it can be used to make calculations easier. Therefore, Equation (3.15) can be rewritten as

$$\mathcal{E}(\rho) = \sum_k \langle e_k|U[\rho \otimes |e_0\rangle\langle e_0|]U^\dagger|e_k\rangle \quad (3.17)$$

$$= \sum_k K_k \rho K_k^\dagger, \quad (3.18)$$

where $K_k \equiv \langle e_k|U|e_0\rangle$ is an operator on the state space of the principal system. The operator-sum representation of \mathcal{E} is given by Equation (3.18). For quantum operation \mathcal{E} , the operators $\{K_k\}$ are known as operation elements or Kraus operators. This representation should be memorized since it will be used many times in this thesis.

The elements of the operation meet a crucial requirement called the completeness relation, similar to the evolution matrices in classical noise. In classical scenarios, this relation comes from the need to make sure probability distributions sum up to one. In the quantum realm, it emerges from a similar need which has to ensure that the trace of $\mathcal{E}(\rho)$ equals one.

$$1 = \text{tr} \mathcal{E}(\rho) \quad (3.19)$$

$$= \text{tr} \left(\sum_k K_k K_k^\dagger \rho \right) \quad (3.20)$$

$$= \text{tr} \left(\sum_k K_k \rho K_k^\dagger \right) \quad (3.21)$$

Because this connection holds for all ρ , it means that we must also have

$$\sum_k K_k^\dagger K_k = I \quad (3.22)$$

This equation works for quantum operations that preserve trace. There are also quantum operations that don't preserve trace, but they will not be discussed further in this project. There are many well-known quantum operations in the academic

resources of quantum information. Amplitude damping is one of them, and it is interesting to review for this project.

3.1.5 Amplitude Damping

In quantum operations, energy dissipation accounts for the effects of energy loss from a quantum system. Whether it is the spontaneous emission of a photon from an atom, a spin system reaching equilibrium at high temperature with its surroundings, or the behavior of a photon in an interferometer or cavity under scattering and attenuation, each process exhibits distinct properties. Nevertheless, they all share a common behavior described by a quantum operation known as amplitude damping. Consider a single optical mode containing the quantum state $\alpha|0\rangle + \beta|1\rangle$, a superposition of zero and one photon. By imagining inserting a partially silvered mirror, a beam splitter, in the path of the photon, can be used to model the scattering of a photon from this mode. The photon is allowed to couple to another single optical mode by the beam splitter, according to the unitary transformation $B = \exp[\theta(a^\dagger b - ab^\dagger)]$, where a, a^\dagger and b, b^\dagger are annihilation and creation operators for photons in the two modes. The output after the beam splitter, assuming the environment starts out with no photons, is $\alpha|00\rangle + \beta \cos \theta |01\rangle + \beta \sin \theta |10\rangle$. Tracing over the environment provides the quantum operation

$$\mathcal{E}_{\text{AD}}(\rho) = K_0 \rho K_0^\dagger + K_1 \rho K_1^\dagger, \quad (3.23)$$

where $K_k = \langle k|B|0\rangle$ are

$$K_0 = \begin{bmatrix} 1 & 0 \\ 0 & \sqrt{1-\gamma} \end{bmatrix} \quad (3.24)$$

$$K_1 = \begin{bmatrix} 1 & \sqrt{\gamma} \\ 0 & 0 \end{bmatrix} \quad (3.25)$$

where $\gamma = \sin^2 \theta$ can be thought of as the probability of losing a photon.

3.1.6 Fidelity between quantum channels

To quantify how well the QRP processor can simulate a desired channel we need a fidelity between the channels. In the simplest case of two unitaries, the fidelity between them is defined to be the average fidelity of their outputs on randomly chosen input states:

$$F(u_1, u_2) = \int d|\phi\rangle |\langle \psi_1 | \psi_2 \rangle|^2 \quad (3.26)$$

$$= \int d|\phi\rangle \langle \phi | U_1^\dagger U_2 | \phi \rangle^2 \quad (3.27)$$

$$F = \frac{1}{n(n+1)} \left\{ \text{Tr} \left(\sum_k M_k^\dagger M_k \right) + \sum_k |\text{Tr}(M_k)|^2 \right\}, \quad (3.28)$$

Line Hjortshøj Pedersen and Niels Martin Møller [30] present a methodology for computing fidelity between a unitary and a general quantum channel. The average fidelity equation is described by Equation (3.28), where $M_k = O^\dagger K_k$, $\{K_k\}$ are the Kraus operators for the map g and O is the unitary transformation.

As mentioned in section 3.1.2, Equation (3.13) characterizes the fidelity between two quantum states. However, for the general quantum channels, the way to calculate the fidelity is slightly different. Once the output state is known, it can be compared with the computational qubit of QRP, and then by repeating this step many times, an average fidelity can be obtained. The most general “fidelity between quantum channel” reads:

$$\frac{1}{n} \sum_i^n F(\rho_{\text{ideal}}^i, \rho_{\text{QRP}}^i) = \frac{1}{n} \sum_i^n \left(\text{tr} \sqrt{\sqrt{\rho_{\text{ideal}}^i} \rho_{\text{QRP}}^i \sqrt{\rho_{\text{ideal}}^i}} \right)^2 \quad (3.30)$$

where ρ_{ideal}^i denotes the output quantum state from the quantum channel, ρ_{QRP}^i denotes the state of the computational qubit of QRP and i refers to the iteration. The input states of these operations are chosen uniformly at random.

3.2 QRP scenario

The following protocol is used for inducing quantum operations on the computational qubits. First, at time $t = 0$, the qubits are initialised. The initial states $|\psi_{in}\rangle$ are sampled uniformly randomly with an assumption that the QN initially begins in the vacuum state $|\text{vac}\rangle_R$. The entire system evolves to a specific time as $t = \tau$, which aligns with a unitary operator $U = \exp[-\frac{iH\tau}{\hbar}]$. The final state of the combined system is thus given by $|\psi_{out}\rangle = U|\psi_{in}\rangle \otimes |\text{vac}\rangle_R$. At the end, the final state of the qubits is described as $\rho_q = \text{Tr}_R[|\psi_{out}\rangle\langle\psi_{out}|]$.

3.2.1 1-qubit reservoir

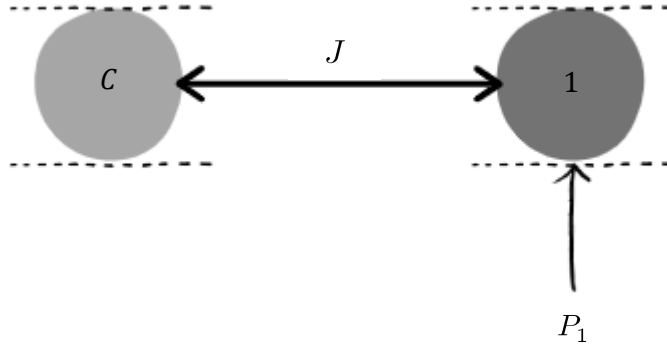


Figure 3.4 The framework of the 1-qubit reservoir. The node C represents the computational qubit and the node 1 represents reservoir qubit.

The objective is to utilize the QRP for showcasing the parametric amplifier and subsequently validating the outcomes against the theoretical predictions. Presently, a singular-node reservoir is being devised to engage with a computational qubit (designated as node C). Within the reservoir, there exists an additional qubit, node 1, and its initial state is the ground state $|g\rangle$. The computational qubit begins in a random state $|\psi\rangle$. There exists a coupling weight J between the qubits. Finally, a pump is added into node 1, introducing an additional parameter into the system.

Eqn. 2.2 can be implemented in the present case, and it becomes

$$H = J(a_1 a_2^\dagger + a_1^\dagger a_2) + E_2 a_2^\dagger a_2 + P a_2^\dagger + P^* a_2, \quad (3.29)$$

Here E_2, P_2 are energy and driving strength respectively. The state $|\psi\rangle$ of the whole system after time t is $|\psi_t\rangle = U|\psi\rangle |g\rangle$, and the final state of the computational qubit is

$$\rho = \langle g|U|g\rangle\rho_0\langle g|U^\dagger|g\rangle + \langle e|U|g\rangle\rho_0\langle g|U^\dagger|e\rangle. \quad (3.30)$$

By looking at this process, the pure state $\rho_0 = |\psi\rangle\langle\psi|$ is mapped to the final state ρ .

One can use eqn. 2.2.3 to calculate the fidelity, with the Kraus operators in this case: $K_1 = \langle g|U|g\rangle$ and $K_2 = \langle e|U|g\rangle$.

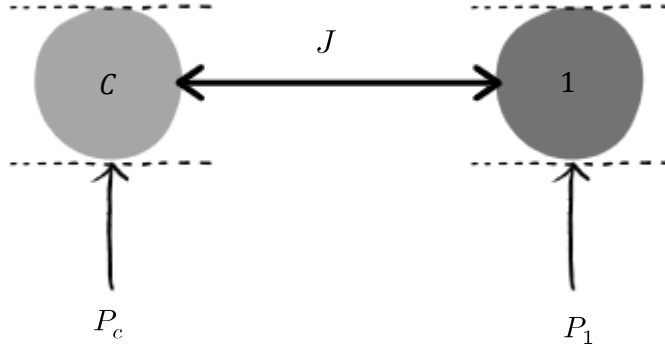


Figure 3.5 The framework of the 1-qubit reservoir by introducing one more pump into the computational qubit C.

Introducing one more pump to the computational node, as illustrated in Figure 3.5, will result in a modification of the Hamiltonian.

$$H = E_1 a_1^\dagger a_1 + P_1 a_1^\dagger + P_1^* a_1 + E_c a_c^\dagger a_c + P_c a_c^\dagger + P_c^* a_c + J(a_1 a_c^\dagger + a_c a_1^\dagger), \quad (3.31)$$

This increases the number of parameters and enhances the fidelity. Since this only adds a term into the Hamiltonian, the derivation is totally same as in the previous part. The same method can be used to calculate the fidelity, just with changed Hamiltonian in Equation (3.29) to Equation (3.31).

3.2.2 2-qubit reservoir

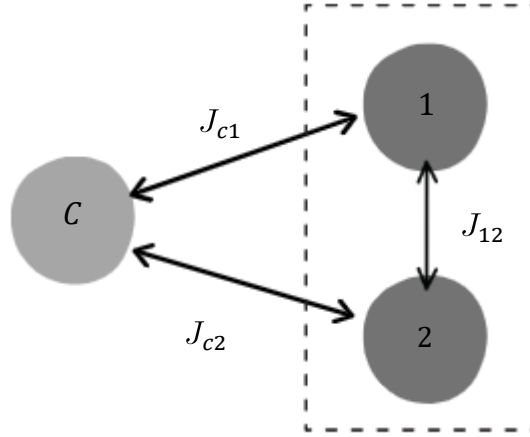


Figure 3.6 The framework of the 2-qubit reservoir. Which is added on one more reservoir qubit from the framework of 1-qubit reservoir.

Now, an additional qubit is introduced into the reservoir, causing the computational qubit C to interact with both qubit nodes 1 and 2. The parameters involved include the coupling constants J_{12} , J_{c1} , J_{c2} , and the pump P_1, P_2 . The complete Hamiltonian (from Equation 2.2) is as follows:

$$\begin{aligned}
 H = & E_1 a_1^\dagger a_1 + P_1 a_1^\dagger + P_1^* a_1 + E_2 a_2^\dagger a_2 + P_2 a_2^\dagger + P_2^* a_2 & (3.32) \\
 & + J_{12}(a_1 a_2^\dagger + a_1^\dagger a_2) + J_{c1}(a_1 a_c^\dagger + a_c a_1^\dagger) \\
 & + J_{c2}(a_c a_2^\dagger + a_c^\dagger a_2) + E_c a_c^\dagger a_c.
 \end{aligned}$$

The initial state of the computational qubit is $|\psi\rangle$ and the two qubits in the reservoir are in their ground states

$$|\psi_0\rangle = |\psi\rangle|00\rangle. \quad (3.33)$$

This state is mapped to,

$$[\rho_t] = \Lambda[\rho] = \text{Tr}_R[U|\psi_0\rangle\langle\psi_0|U^\dagger], \quad (3.34)$$

By expanding this,

$$\begin{aligned}
 \rho_t = & \langle 00|U|\psi_0\rangle\langle\psi_0|U^\dagger|00\rangle + \langle 01|U|\psi_0\rangle\langle\psi_0|U^\dagger|01\rangle & (3.35) \\
 & + \langle 10|U|\psi_0\rangle\langle\psi_0|U^\dagger|10\rangle + \langle 11|U|\psi_0\rangle\langle\psi_0|U^\dagger|11\rangle,
 \end{aligned}$$

$$\begin{aligned}
 \rho_t = & \langle 00|U|00\rangle\rho_0\langle 00|U^\dagger|00\rangle + \langle 01|U|00\rangle\rho_0\langle 00|U^\dagger|01\rangle + & (3.36) \\
 & \langle 10|U|00\rangle\rho_0\langle 00|U^\dagger|10\rangle + \langle 11|U|00\rangle\rho_0\langle 00|U^\dagger|11\rangle,
 \end{aligned}$$

The corresponding Kraus operators are given by

$$K_{00} = \langle 00|U|00\rangle, \quad (3.37a)$$

$$K_{01} = \langle 01|U|00\rangle, \quad (3.37b)$$

$$K_{10} = \langle 10|U|00\rangle, \quad (3.37c)$$

$$K_{11} = \langle 11|U|00\rangle, \quad (3.37d)$$

3.3 Optimization algorithm

3.3.1 Training of unitary

Training of the quantum neural network is an optimization process. All the parameters, defined as a matrix S_{kl} are being optimised. These parameters will be assumed to be within a certain interval and are expected to produce fidelity close to one. In the training of unitary, the situation is relatively simple with a small number of parameters. A deterministic method, Nelder-Mead simplex algorithm is considered sufficient to be implemented in order to approach the optimum condition. It should be mentioned that the Scipy library of Python contains the Nelder-Mead simplex algorithm and it has been widely used, hence it will be utilized directly for this purpose.

3.3.2 Training of channels

Since there is no closed-form expression for the fidelity between quantum channels, a stochastic genetic algorithm is implemented to find the optimum condition starting from a set of initial guesses, which approach the optimum point in a random process.

The genetic algorithm is an optimization algorithm imitating biological evolution with the principle of natural selection. Initially, a random set of numbers is described as a population, which goes through a natural selection procedure according to a fitness criterion. The fittest individuals, which literally means the set of parameters that produce the best result, reproduce to the next generation of populations through a cross-breeding procedure. A random mutation is allowed to happen with certain probability, which ensures the diversity among the populations.

Flow of the genetic algorithm

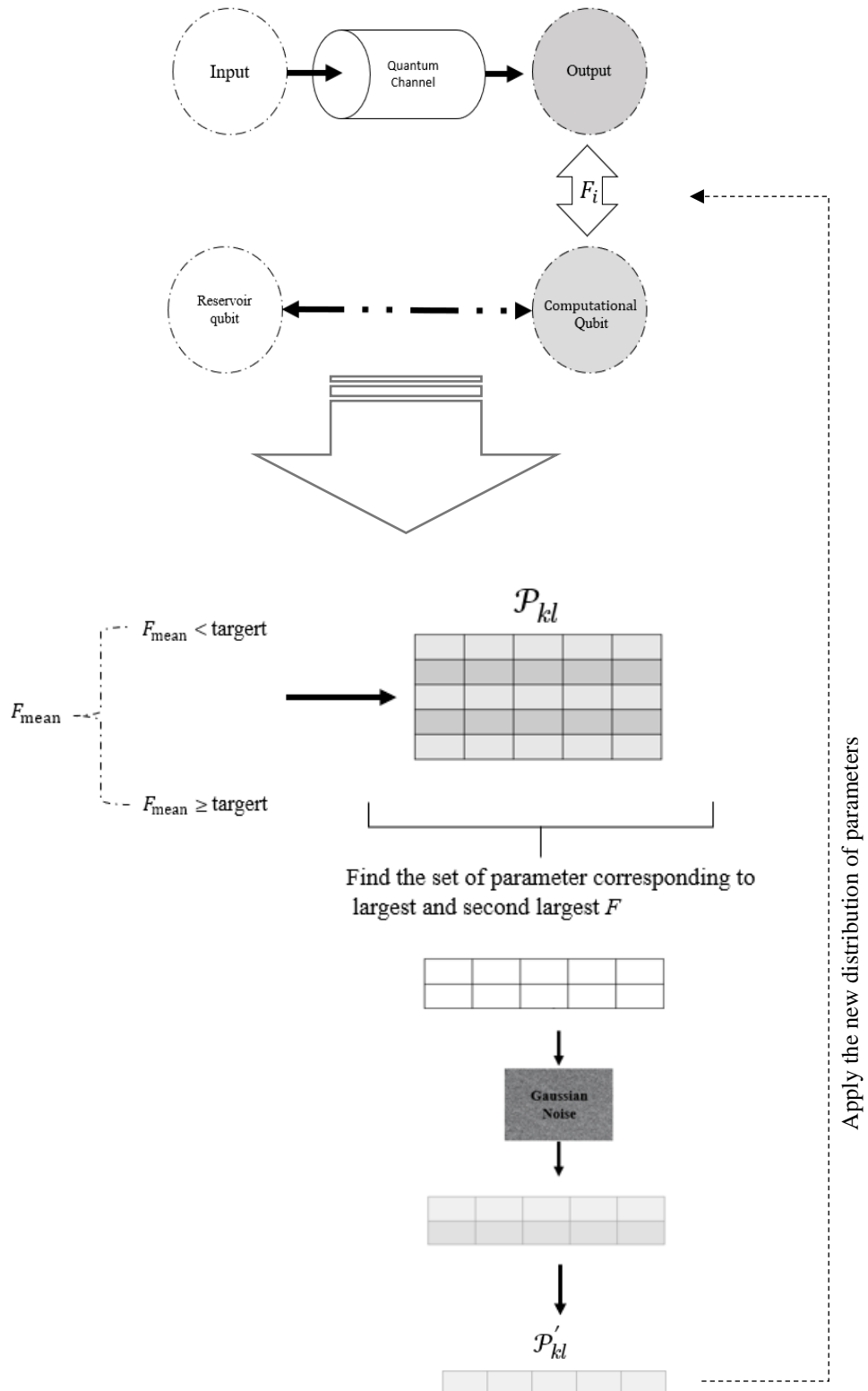


Figure 3.7 The flow of the genetic algorithm, the entire algorithm begins from left hand side and it flows as a circle until the terminate condition F_{mean} is reached

Figure 3.7 illustrates the flow of the genetic algorithm. The following steps describe it:

- i) A set of random numbers in a given interval is randomly generated by the computer. The range of parameters depends on the complexity of the Hamiltonian.
- ii) The computer is asked to generate a random quantum state in 2 dimensions, and then the quantum state will be input into the quantum channel to get the ideal output ρ_{ideal} , i.e. the desired output.
- iii) The QRP scenario, as shown in section 3.2, is run producing an evolved quantum state, which is denoted ρ_{QRP} . Fidelity between quantum channels is then computed and saved at this moment.
- iv) Repeat step iii) $i = 100$ times, and take an average from fidelities F_i , denoted as F_{mean} .
- v) Find the largest and second largest values, defined as $F_{1\text{st}}$ and $F_{2\text{nd}}$ from F_i and its corresponding parameter set.
- vi) Compute next generation of parameters as:

$$\mathcal{P}'_{kl} = \frac{(\mathcal{P}_{kl}^p + \mathcal{P}_{kl}^q)}{2} + \delta N(x), \quad (3.38)$$

where δ is the mutation rate, $N(x)$ is the noise, which is chosen as a gaussian distribution.

- vii) Replace the initial guess by \mathcal{P}'_{kl} , and repeat step ii) – vi) until F_{mean} approaches to a target value F_a . In other words, F_a is the expected accuracy in QRP simulation.

The resulting \mathcal{P}'_{kl} will be the best parameters, i.e. providing the simulation accuracy F_a . In general, the closer F_{mean} to 1, the closer the simulation to the ideal operation.

CHAPTER 4

RESULTS

In this section, the results of the simulations will be presented. First by giving the results using the Nelder-Mead algorithm for optimisation, and later using the genetic algorithm. The section starts with simple cases and the complexity increases while reading. All the data is obtained for a single computational qubit.

4.1 Implementation of unitary

Consider first the case of unitary operations, i.e. we would like the QRP processor to learn any unitary map. It turns out this is possible, but before we show those general results, let us present the data for the set of unitaries that can be used to approximate any single-qubit unitary.

4.1.1 Simple unitary operations

Since the space of quantum states of a single qubit is isomorphic to a sphere and a set of 2x2 unitaries to rotations in 3D, we first show how to implement basic rotations such as those represented by Pauli matrices and other simple gates, see Fig. 4.1.

Hadamard	$\text{---}[H]\text{---}$	$\frac{1}{\sqrt{2}} \begin{bmatrix} 1 & 1 \\ 1 & -1 \end{bmatrix}$
Pauli-X	$\text{---}[X]\text{---}$	$\begin{bmatrix} 0 & 1 \\ 1 & 0 \end{bmatrix}$
Pauli-Y	$\text{---}[Y]\text{---}$	$\begin{bmatrix} 0 & -i \\ i & 0 \end{bmatrix}$
Pauli-Z	$\text{---}[Z]\text{---}$	$\begin{bmatrix} 1 & 0 \\ 0 & -1 \end{bmatrix}$
Phase	$\text{---}[S]\text{---}$	$\begin{bmatrix} 1 & 0 \\ 0 & i \end{bmatrix}$
$\pi/8$	$\text{---}[T]\text{---}$	$\begin{bmatrix} 1 & 0 \\ 0 & e^{i\pi/4} \end{bmatrix}$

Figure 4.1 Pauli matrices and simple gates

Table 4.1 shows the fidelity histograms of QRP optimization for the following single-qubit unitaries depicted in Fig. 4.1.

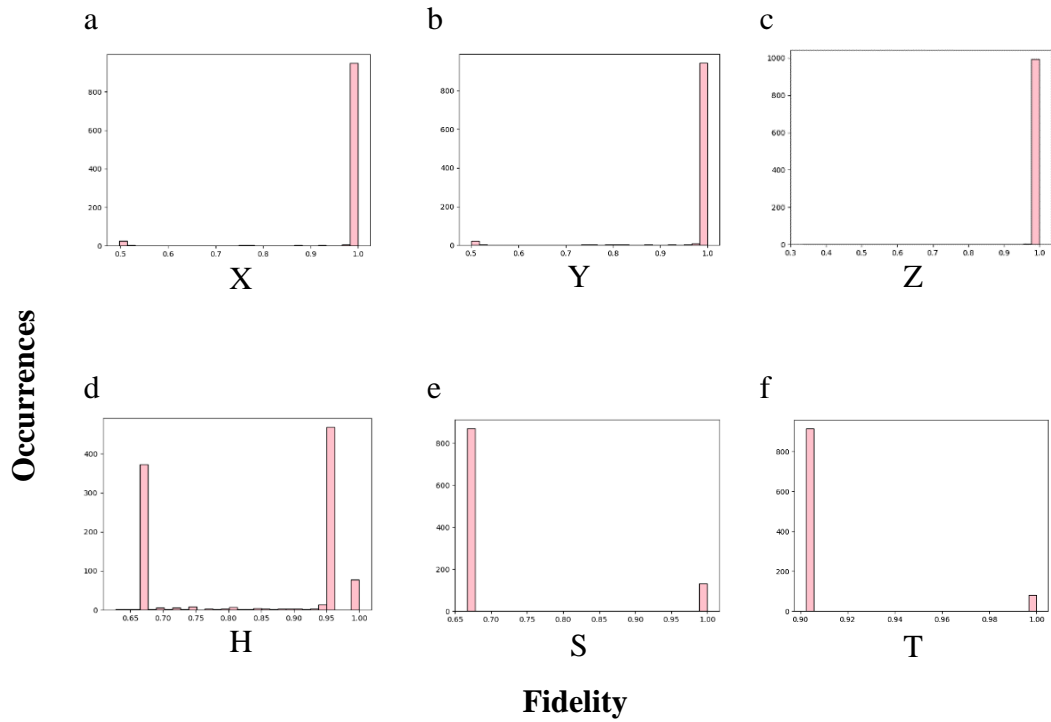


Table 4.1 The histogram of fidelity of the unitary mentioned below the plot. See Fig. 4.1 for concrete formulae.

The results show that for each gate, the Nelder algorithm can obtain a very good parameter set.

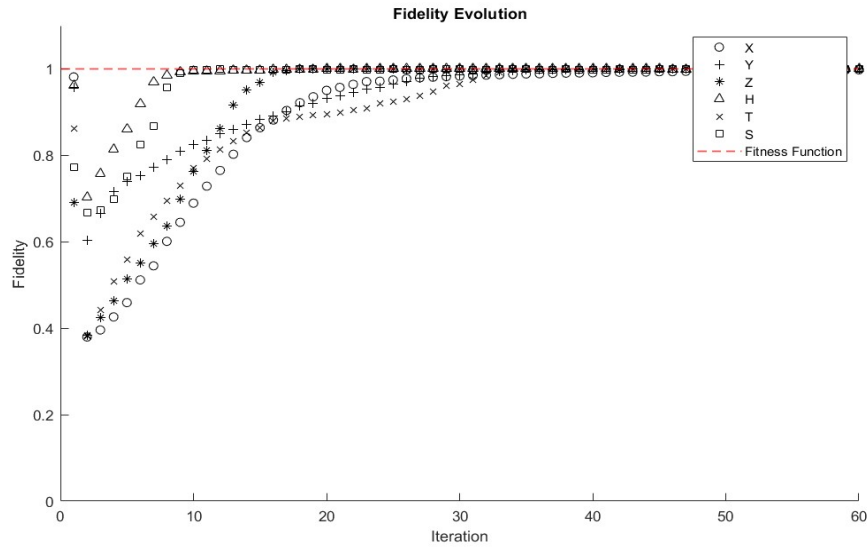


Figure 4.2 The implementation of genetic algorithm to learn a unitary transformation. The plot gives the evolution of the fidelity in terms of iterations of the algorithm.

The genetic algorithm was also used for the purpose of simulating the unitary gates. The results are shown in Fig. 4.2. The first iteration returns a low fidelity due to the random guess of the parameters set, but after several iterations, the fidelities keep increasing and converge at fidelity close to 1, which is the fitness criterion.

By comparing Table 4.1 and Fig. 4.2, the Nelder's algorithm and genetic algorithms provide similar optimization results, i.e. they are both able to find very good parameter sets.

4.1.2 Random unitaries

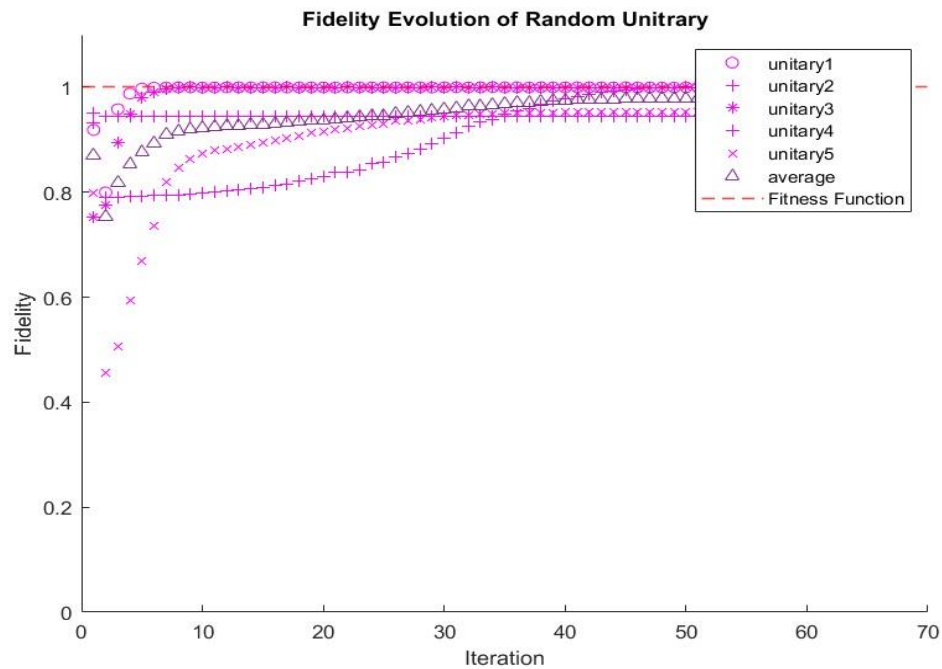


Figure 4.3 The optimization process of random unitary transformation with 1-qubit reservoir. The fidelities change during each optimization and the triangle curve is the average from 5 unitaries.

Consider now an arbitrary unitary. The simulation by QRP is more challenging as shown in Fig. 4.3. By comparing the evolution trends of five random unitary matrices and taking an average of them, it shows that the average fidelity can evolve from a random guess to a value that is very close to the fitness criterion. This data shows that QRP is capable of learning any unitary transformation. To sum up, Fig. 4.3 shows the optimization by genetic algorithm for random unitaries and they all can be implemented by QRP with very good fidelities.

4.1.3 Comparison between 1-qubit and 2-qubit reservoir

It is intriguing to study whether the performance improves as the structure of the reservoir becomes more complex. The same set of unitaries was also analysed with 2-qubit reservoir with the Nelder-Mead algorithm.

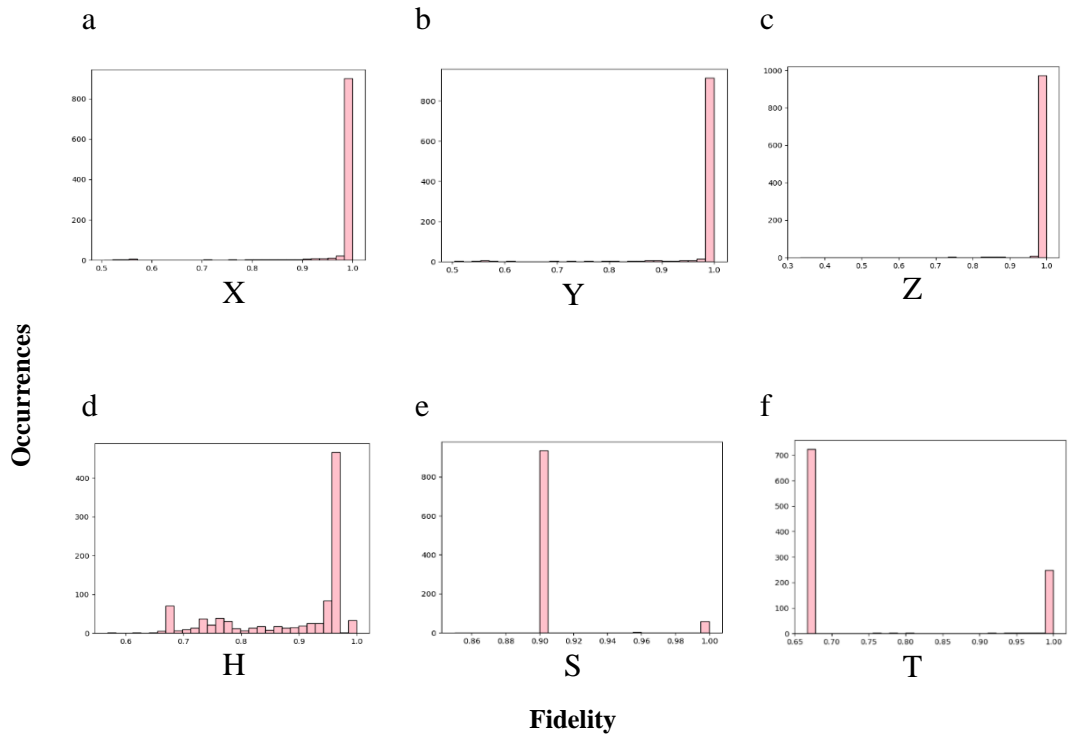


Table 4.2 The optimization process (Nelder algorithm) of simple unitary transformations with 2-qubit reservoir. Each diagram represents the fidelity histogram.

Table 4.2 shows the fidelity histograms for different unitaries. The result is similar to Table 4.1, but 4.2 (d) and (e) show that the chance to find the best parameters is lower for the two-qubit QRP.

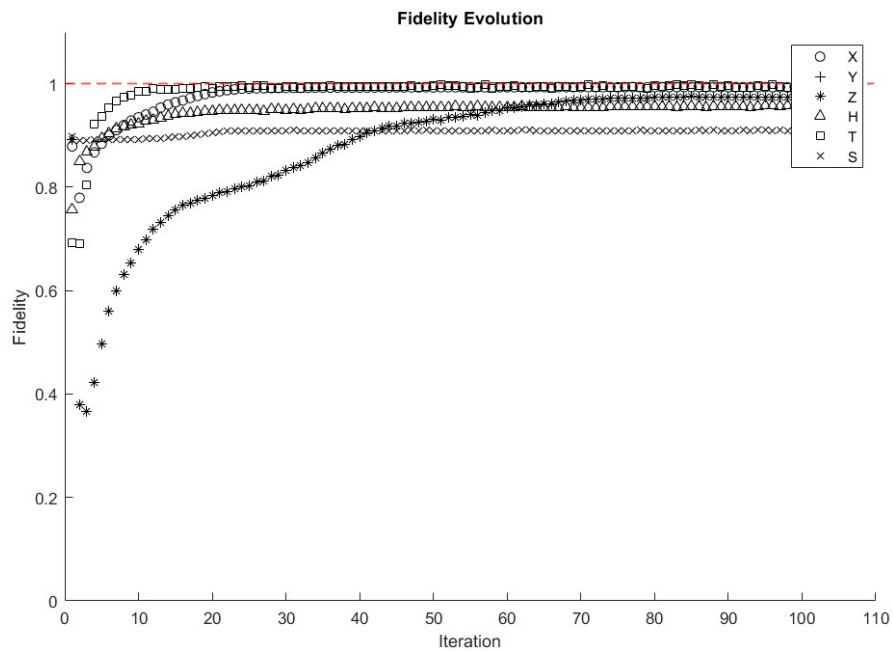


Figure 4.4 The optimization process of simple unitary transformations with 2-qubit reservoir. The dashed line represents the ideal value.

The same set of unitaries was also analysed with 2-qubit reservoir with the genetic algorithm.

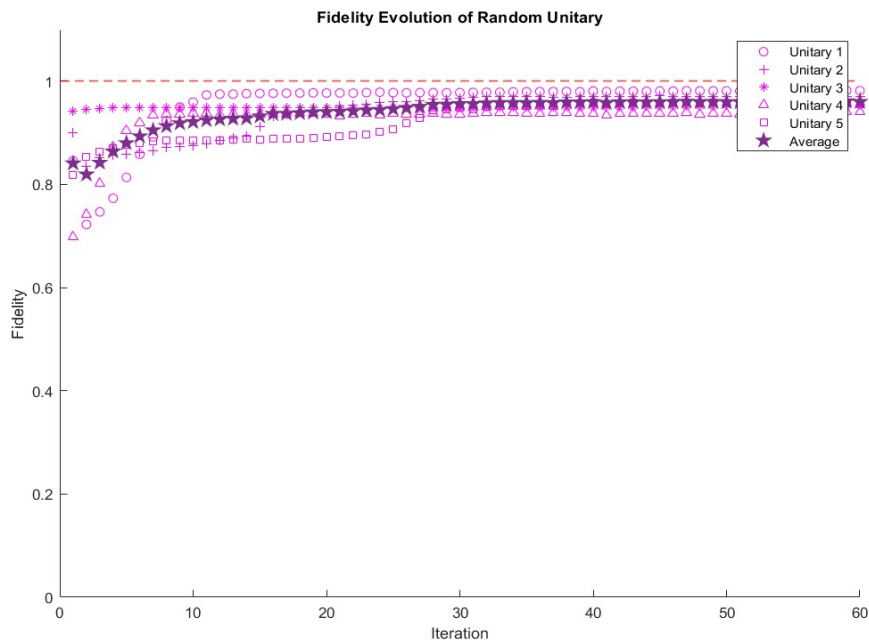


Figure 4.5 The optimization process of random unitary transformation with 2-qubit reservoir. The stars show the average over 5 unitaries.

The data presented in Figs. 4.4 (4.5) shows that a larger (smaller for random unitaries) number of iterations is needed for the 2-qubit reservoir to achieve the same fidelity as the 1-qubit reservoir. Yet, the differences are not that significant.

4.2 Implementation of channels

Now, let's move to more complicated quantum operations and first study the amplitude damping quantum channel. This time the fidelity calculations cannot be done using the Nelder algorithm and instead it has to be resorted to the generic algorithm.

4.2.1 Amplitude damping

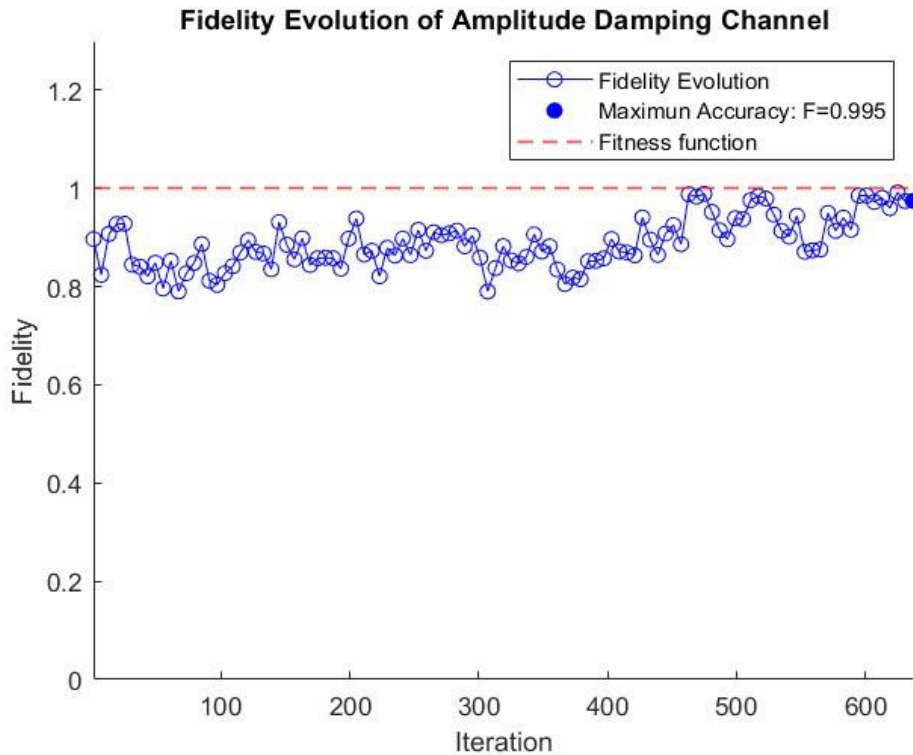


Figure 4.6 The optimization process of QRP in simulating amplitude damping channel.

From now on the reservoir is composed of a single qubit only. Fig. 4.6 shows the channel fidelity evolution as the system is being iterated through the genetic algorithm. The way of training amplitude damping channel as described in section 3.3.2. It was implemented into QRP and Fig. 4.6 shows how QRP approaches the simulation of the amplitude damping channel with a given target accuracy. As seen, the optimization does not always increase fidelity but from time to time the fidelity is decreased. This comes from two factors. Since the parameter sets are generated randomly and affected

by the noises during each iteration, the new parameter set may be not suitable for good results. Secondly, since the input state was sampled randomly for the amplitude damping, this may increase the variable that is uncontrollable, which means the object for QRP to learn behaves more randomly, therefore optimization is more challenging. As an observation, the success of parameter optimization requires some sweet zone, which is a particular upper bound and lower bound on the parameters. For instance,

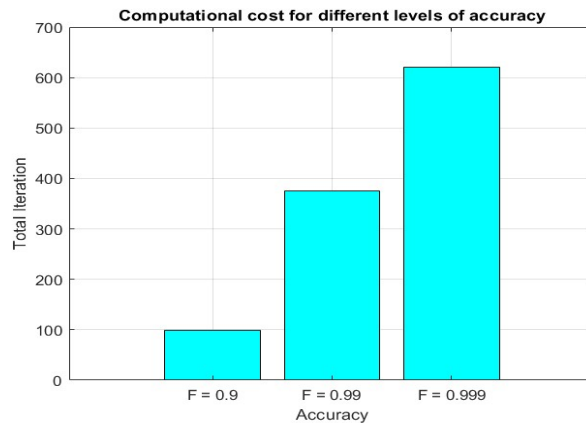


Figure 4.7 The total iterations requirement to achieve a given accuracy, i.e. computational cost.

when the QRP is learning amplitude damping channel, the interval of all parameters lies between -50 and 50, this interval can make the optimization work successfully but other values such as [-1,1], [-100,100], turn out to be not so good.

As mentioned above, the random sampling increases the uncontrollable variable for QRP. Figure 4.7 shows a statistic for different trials of varied target accuracy. It shows that if the target accuracy is raised by requiring fewer rounding decimal points, it requires significantly more iterations. Therefore, it may be concluded that the higher accuracy the higher computational cost for the QRP.

4.2.2 Random channel

To investigate the capability of QRP in learning quantum operations more deeply, a random channel is implemented. Figure 4.8 presents the data collected when QRP simulates a random quantum channel, where the channel was chosen uniformly at random.

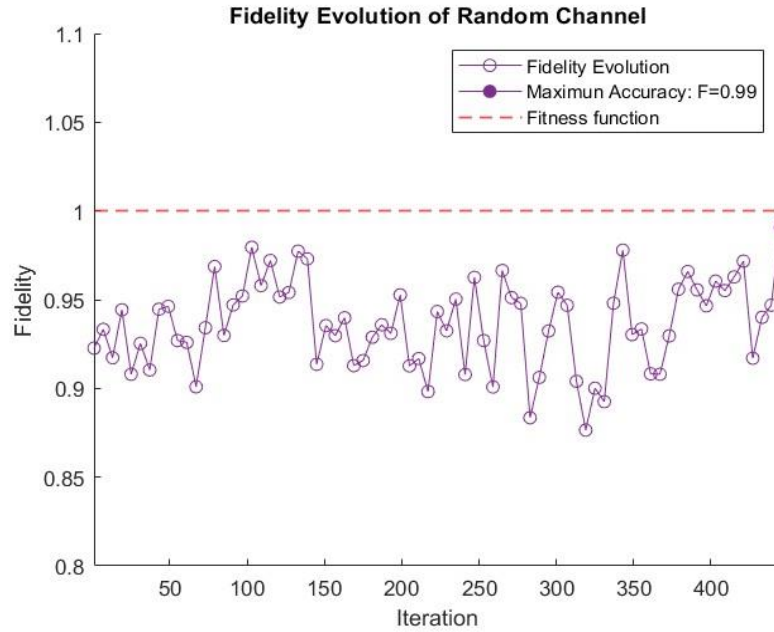


Figure 4.8 Fidelity between random quantum channel and the channel realised by a random choice of parameters in QRP. Since optimisation has not been implemented here, the actual fidelities will be even higher

The result is quite similar to the simulation of amplitude damping. Notice that the maximum fidelity reached is $F = 0.99$. This is good enough since the simulation object is more random compared to amplitude damping. Unlike amplitude damping, in random quantum channels, the Kraus operators keep changing during each iteration increasing the difficulty of finding the suitable interval for optimization, this is another factor to be considered in comparison. It is therefore quite remarkable that QRP is capable of simulating any single-qubit channels.

Hence, the findings from this section collectively demonstrate QRP's capability to adapt and learn various quantum processes effectively.

4.3 Implementation of quantum amplifier

4.3.1 Kraus operator for the parametric amplifier

To simplify the case, assume that the input and output state is in a two-dimensional subspace spanned by $\{|0\rangle, |1\rangle\}$. By using the number basis from the parametric amplifier, see Equation (2.28), the Kraus operator K_0 reads:

$$K_0 = \langle 0|S(r)|0\rangle = \frac{1}{g}g^{-a^\dagger a}, \quad (4.1)$$

Since $g^x = e^{\ln g x}$, Taylor's expansion gives:

$$K_0 = \frac{1}{g} I - \ln g a^\dagger a + \frac{1}{2}\ln^2 g a^\dagger a^2 + \dots, \quad (4.2)$$

for the values of gain g close to 1.

The terms of higher power can be ignored since their value is pretty small, so that

$$K_0 = \frac{1}{g} \begin{pmatrix} 1 & 0 \\ 0 & 1 - \ln g + \frac{1}{2}\ln^2 g \end{pmatrix}, \quad (4.3)$$

Similarly,

$$K_1 = \langle 1|S(r)|0\rangle = \frac{-1}{g} \sqrt{g^2 - 1} g^{-a^\dagger a} a^\dagger, \quad (4.4)$$

$$= \sqrt{1 - 1/g^2} \begin{pmatrix} 0 & 0 \\ 1 - \ln g + \frac{1}{2}\ln^2 g & 0 \end{pmatrix}, \quad (4.5)$$

where a and a^\dagger are annihilation operator and creation operator correspondingly reduced to the two-dimensional subspace. Ideally, the Kraus operators should satisfy

$$K_0^\dagger K_0 + K_1^\dagger K_1 = I, \text{ (ideally)} \quad (4.6)$$

but due to our assumptions this condition holds only approximately as we now explain.

4.3.2 The gain parameter

Since $K_0(g)$ and $K_1(g)$ are the function of g , where g is the gain of the input state which is expected to be amplified, from calculation it is observed that Equation (4.8) is not perfectly identity but has a linear relationship with g . The current result shows that the approximation of parametric amplifier does not hold for large gain. Indeed, to keep $K_0^\dagger K_0 + K_1^\dagger K_1 \approx I$, the diagonal elements should be $I_{00}, I_{11} \approx 1$. Fig. 4.3.2 shows them as a function of g , indicating that g can be larger than 1 only by less than 1/100.

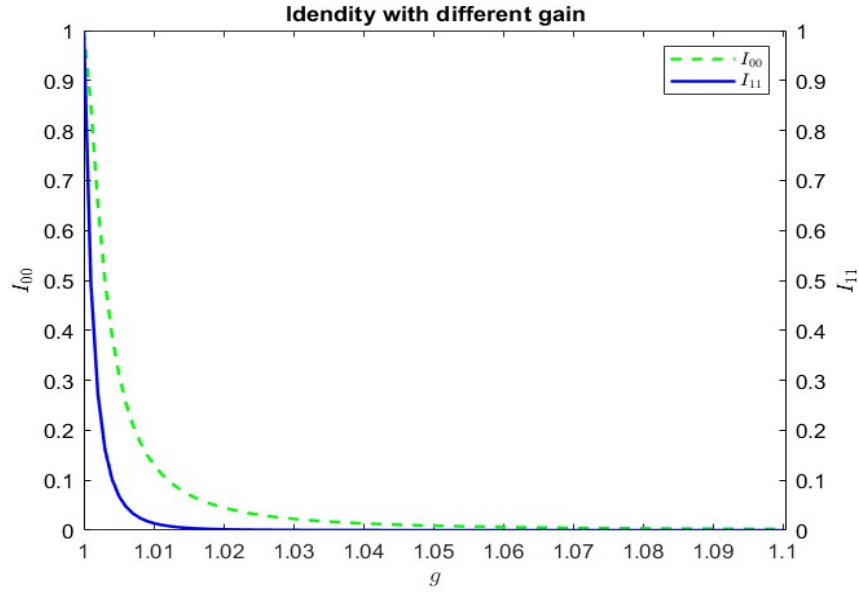


Figure 4.9 The diagonal elements of $K_0^\dagger K_0 + K_1^\dagger K_1$ in the two-dimensional approximation of the parametric amplifier.

4.3.3 Fidelity of the amplifier map

By choosing $g < 1.01$, $K_0^\dagger K_0 + K_1^\dagger K_1$ is approximately an identity and we have a proper Kraus decomposition. Therefore, Equation (3.30) can be used to compute the fidelity of this map with the upcoming QRP map.

4.3.4 QRP implements parametric amplifier

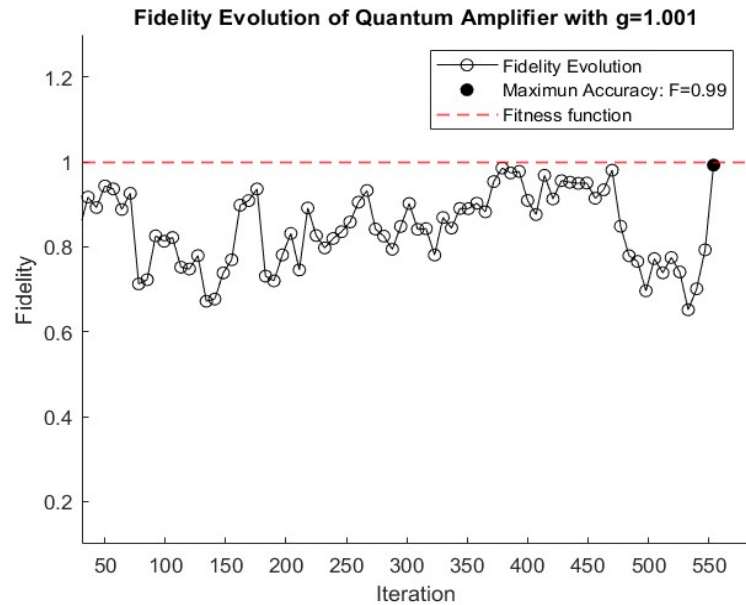


Figure 4.10 The optimization process of QRP in simulating parametric amplifier with $g = 1.001$. The circles show every 6th element of the evolving data. The solid circle is the maximal achieved accuracy.

To demonstrate the QRP learning capability of quantum amplifier, the random sampling method mentioned in Section 3.3.2 is first implemented.

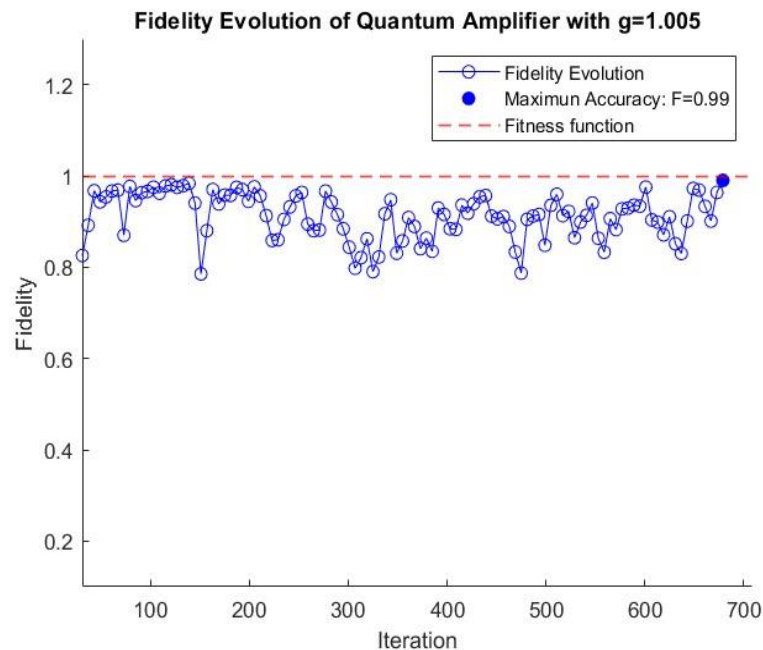


Figure 4.11 The optimization process of QRP simulating parametric amplifier with $g = 1.005$. The circles show every 6th element of the evolving data. The filled solid circle is the maximum accuracy achieved.

Figure 4.9 and 4.10 shows the learning process of QRP when simulating quantum amplifier. During this process, the set of random states are sampled into the amplifier and the QRP is forced to learn from this operation. The maximum accuracy is limited at fidelity $F = 0.99$. As the result shows, the larger expected gain requires more computational steps, but the fluctuation is much smaller compared to the small gain. It can be concluded that QRP is capable of implementing the amplifier.

CHAPTER 5

DISCUSSION

It was shown that QRP is a versatile platform for implementing many general quantum channels. A particularly interesting one is the quantum amplifier. In this case the platform behaves as expected (fidelity is above 0.99) but at present the whole theory is restricted to the gain of less than 1/100. This is clearly not satisfactory from an experimental point of view and should be overcome. The two points that should be improved are as follows: (i) consider higher-dimensional Kraus operators and (ii) consider more terms in the expansion of the Kraus operators in terms of the gain g . This will definitely be done in the future.

Another major limitation of this thesis is the restriction to single computational qubit and, in most of the calculations, to only a single qubit in the reservoir. More work is required to understand the scaling of performance of QRP with the additional nodes in the quantum network. Intuitively one expects that the performance can only improve, but some of our preliminary data shows to the contrary, indicating need for clarification.

CHAPTER 6

CONCLUSION AND RECOMMENDATION

In this thesis, the feasibility of utilizing Quantum Reservoir Processors (QRPs) to realize quantum-limited amplifiers has been explored, addressing a significant challenge in quantum information technologies. The primary motivation was to enhance weak quantum signals for efficient transmission over long distances, a task constrained by the no-cloning theorem and the Haus-Caves limit.

Through a comprehensive review of quantum amplifier theory and its operational principles, a foundational understanding of quantum channels and Kraus operators was established. This theoretical groundwork enabled the development of a robust framework for QRPs, demonstrating their capacity to simulate unitary transformations and quantum channels effectively.

The QRP's conceptual simplicity and universality were pivotal in the approach. By optimizing over a single layer, the QRP's versatility is harnessed to perform multiple measurements, prepare various quantum states, and execute complex computations. The simulations confirmed that QRPs could learn any unitary transformation on a qubit and any quantum channel on a qubit with high efficiency.

The findings in this thesis underscore the potential of QRPs to serve as practical tools for simulating quantum-limited amplifiers. The ability to predict time evolution in nonlinear dynamics and chaotic systems further highlights the QRP's applicability beyond quantum amplification, suggesting broader applications in both classical and quantum domains.

In conclusion, this research paves the way for the development of physical quantum amplifying devices, leveraging QRP's unique advantages. Future work may focus on experimental implementations, optimizing QRP architectures for specific amplification tasks, and exploring their integration into larger quantum information systems. The advancements presented in this thesis contribute to the ongoing effort to

bridge quantum theory and practical quantum technologies, moving us closer to realizing efficient, reliable quantum communication networks.

To overcome current limitations, future research should focus on two key improvements: (i) employing higher-dimensional Kraus operators and (ii) including more terms in the Kraus operator expansions in relation to the gain g . Additionally, expanding the study to involve more computational qubits and larger reservoirs is essential. Investigating the scaling of QRP performance with increased network nodes is crucial, as preliminary data indicates potential complexities that need clarification. These steps will enhance the practical applicability and efficiency of QRPs in quantum amplification and other advanced quantum information processing tasks.

REFENRECES

- [1] Clerk, A. A., Devoret, M. H., Girvin, S. M., Marquardt, F., & Schoelkopf, R. J. (2010). Introduction to Quantum Noise, Measurement, and Amplification. *Reviews of Modern Physics*, 82(2), 1155-1208. <https://doi.org/10.1103/RevModPhys.82.1155>, (n.d.).
- [2] Caves, C. M. (1982). Quantum Limits on Noise in Linear Amplifiers. *Physical Review D*, 26(8), 1817-1839. <https://doi.org/10.1103/PhysRevD.26.1817>, (n.d.).
- [3] Bergeal, N., Schackert, F., Metcalfe, M., Vijay, R., Manucharyan, V. E., Frunzio, L., Prober, D. E., Schoelkopf, R. J., Girvin, S. M., & Devoret, M. H. (2010). Phase-Preserving Amplification near the Quantum Limit with a Josephson Ring Modulator. *Nature*, 465(7294), 64–68. <https://doi.org/10.1038/Nature09035>, (n.d.).
- [4] Metelmann, A., Lanes, O., Chien, T.-Z., McDonald, A., Hatridge, M., & Clerk, A. A. (2022). Quantum-Limited Amplification without Instability. *arXiv*. <https://arxiv.org/abs/2208.00024>, (n.d.).
- [5] Krisnanda, T., Ghosh, S., Paterek, T., Laskowski, W., & Liew, T. C. H. (2022). Phase Measurement beyond the Standard Quantum Limit Using a Quantum Neuromorphic Platform. *Physical Review Applied*, 18(3), 034011. <https://doi.org/10.1103/PhysRevApplied.18.034011>, (n.d.).
- [6] Ghosh, S., Opala, A., Matuszewski, M., Paterek, T., & Liew, T. C. H. (2019). Quantum Reservoir Processing. *NPJ Quantum Information*, 5(1), 35. <https://doi.org/10.1038/S41534-019-0149-8>, (n.d.).
- [7] Biamonte, J., Wittek, P., Pancotti, N., Rebentrost, P., Wiebe, N., & Lloyd, S. (2017). Quantum Machine Learning. *Nature*, 549(7671), 195-202. <https://doi.org/10.1038/Nature23474>, (n.d.).
- [8] Dunjko, V., & Briegel, H. J. (2018). Machine Learning & Artificial Intelligence in the Quantum Domain: A Review of Recent Progress. *Reports on Progress in Physics*, 81(7), 074001. <https://doi.org/10.1088/1361-6633/Aab406>, (n.d.).
- [9] Altaisky, M. V., Kaputkina, N. E., Krylov, S. Yu., & Es'kov, V. A. (2016). Towards a Feasible Implementation of Quantum Neural Networks Using

- Quantum Dots. *Applied Physics Letters*, 108(10), 103108.
<https://doi.org/10.1063/1.4943659>, (n.d.).
- [10] Stajic, J., Stone, R., Chin, G., & Wible, B. (2015). Rise of the Machines. *Science*, 349(6245), 248-249. <https://doi.org/10.1126/Science.349.6245.248>, (n.d.).
- [11] Chouard, T., & Venema, L. (2015). Machine Intelligence. *Nature*, 521(7553), 435. <https://doi.org/10.1038/521435a>, (n.d.).
- [12] LeCun, Y., Bengio, Y., & Hinton, G. (2015). Deep Learning. *Nature*, 521(7553), 436-444. <https://doi.org/10.1038/Nature14539>, (n.d.).
- [13] Lukoševičius, M. (2012). *A Practical Guide to Applying Echo State Networks*. Berlin, Germany: Springer Berlin Heidelberg., (n.d.).
- [14] Ghosh, S., Opala, A., Matuszewski, M., Paterek, T., & Liew, T. C. H. (2021). Reconstructing Quantum States with Quantum Reservoir Networks. *IEEE Transactions on Neural Networks and Learning Systems*, 32(7), 3148–3155. <https://doi.org/10.1109/TNNLS.2020.3009716>, (n.d.).
- [15] Ghosh, S., Krisnanda, T., Paterek, T., Ruskai, M. B., & Liew, T. C. H. (2021). Realising and Compressing Quantum Circuits with Quantum Reservoir Computing. *Communications Physics*, 4, 105. <https://doi.org/10.1038/S42005-021-00606-3>, (n.d.).
- [16] Ghosh, S., Paterek, T., & Liew, T. C. H. (2019). Quantum Neuromorphic Platform for Quantum State Preparation. *Physical Review Letters*, 123(26), 260404. <https://doi.org/10.1103/PhysRevLett.123.260404>, (n.d.).
- [17] Krisnanda, T., Paterek, T., Paternostro, M., & Liew, T. C. H. (2023). Quantum Neuromorphic Approach to Efficient Sensing of Gravitationally-Induced Phenomena. *Physical Review D*, 107(8), 086014., (n.d.).
- [18] Shimoda, K., Takahasi, H., & Townes, C. H. (1957). Fluctuations in Amplification of Quanta with Application to Maser Amplifiers. *Journal of the Physical Society of Japan*, 12, 686-700. <https://api.semanticscholar.org/CorpusID:121906375>, (n.d.).
- [19] Weber, J. (1959). Masers. *Reviews of Modern Physics*, 31(3), 681-710. <https://doi.org/10.1103/RevModPhys.31.681>, (n.d.).
- [20] Gordon, J. P., Walker, L. R., & Louisell, W. H. (1963). Quantum Statistics of Masers and Attenuators. *Physical Review*, 130(2), 806-812. <https://doi.org/10.1103/PhysRev.130.806>, (n.d.).

- [21] Heffner, H. (1962). The Fundamental Noise Limit of Linear Amplifiers. *Proceedings of the IRE*, 50(7), 1604-1608., (n.d.).
- [22] Clarke, J., Goubau, W.M. & Ketchen, M.B. Tunnel Junction Dc SQUID: Fabrication, Operation, and Performance. *J Low Temp Phys* 25, 99–144 (1976). <https://doi.org/10.1007/BF00654826>, (n.d.).
- [23] Chia, A., Hajdušek, M., Nair, R., Fazio, R., Kwek, L. C., & Vedral, V. (2020, October). Phase-Preserving Linear Amplifiers Not Simulable by the Parametric Amplifier. *Physical Review Letters*, 125(16), 163603. <https://doi.org/10.1103/PhysRevLett.125.163603>, (n.d.).
- [24] Haus, H. A., & Mullen, J. A. (1962, December). Quantum Noise in Linear Amplifiers. *Physical Review*, 128(5), 2407–2413. <https://doi.org/10.1103/PhysRev.128.247>, (n.d.).
- [25] Caves, C. M. (1982, October). Quantum Limits on Noise in Linear Amplifiers. *Physical Review D*, 26(8), 1817–1839. <https://doi.org/10.1103/PhysRevD.26.1817>, (n.d.).
- [26] Mollow, B. R., & Glauber, R. J. (1967, August). Quantum Theory of Parametric Amplification. I. *Physical Review*, 160(5), 1076–1096. <https://doi.org/10.1103/PhysRev.160.1076>, (n.d.).
- [27] Caves, C., Combes, J., Jiang, Z., & Pandey, S. (2012). Quantum Limits on Phase-Preserving Linear Amplifiers. *Physical Review A*, 86(6), (n.d.).
- [28] Collett, M. J., & Walls, D. F. (1988, November). Quantum Limits to Light Amplifiers. *Physical Review Letters*, 61(21), 2442–2444. <https://doi.org/10.1103/PhysRevLett.61.2442>, (n.d.).
- [29] Schumaker, B. L., & Caves, C. M. (1985). New Formalism for Two-Photon Quantum Optics. II. Mathematical Foundation and Compact Notation. *Physical Review A*, 31(5), 3093-3111. <https://doi.org/10.1103/PhysRevA.31.3093>, (n.d.).
- [30] Nielsen, M. A., & Chuang, I. L. (2000). *Quantum Computation and Quantum Information*. Cambridge University Press., (n.d.).
- [31] K. Kraus, in *States, Effects, and Operations: Fundamental Notions of Quantum Theory*, Springer Lecture Notes in Physics Vol. 190 (Springer-Verlag, Berlin, 1983), (n.d.).
- [32] Nha, H., Milburn, G. J., & Carmichael, H. J. (2010). Linear Amplification and Quantum Cloning for Non-Gaussian Continuous Variables. *New Journal of*

Physics, 12(10), 103010. <https://doi.org/10.1088/1367-2630/12/10/103010>,
(n.d.).

- [33] Jozsa, R. (1994). Fidelity for Mixed Quantum States. *Journal of Modern Optics*, 41(12), 2315-2323. <https://doi.org/10.1080/09500349414552171>, (n.d.).